CHAPTER 3. LABORATORY FOURIER TRANSFORM INFRARED SPECTROSCOPY METHODS FOR GEOLOGIC SAMPLES

P.L. King[1], M.S. Ramsey[2], P.F. McMillan[3, 4], & G. Swayze[5]
[1] Department of Earth Sciences,
University of Western Ontario,
London ON N6A 5B7 Canada
penny.king@uwo.ca

[2] Department of Department of Geology & Planetary Science,
University of Pittsburgh,
Pittsburgh, PA 15260-3332, USA

[3] Department of Chemistry,
Christopher Ingold Laboratories,
University College London,
London WC1H 0AJ, United Kingdom

[4] Davy-Faraday Research Laboratory,
Royal Institution of Great Britain,
London W1X 4BS, United Kingdom

[5] U.S. Geological Survey,
MS 964 Box 25046,
Denver Federal Center,
Denver, CO 80225, USA

INTRODUCTION

Fourier Transform Infrared (FTIR) spectroscopy is a technique used to determine qualitative and quantitative features of IR-active molecules in organic or inorganic solid, liquid or gas samples. It is a rapid and relatively inexpensive method for the analysis of solids that are crystalline, microcrystalline, amorphous, or films. Samples are analyzed on the scale of microns to the scale of kilometers and new advances make sample preparation, where needed, relatively straight-forward. Another advantage of the IR technique is that it also can provide information about the "light elements" (*e.g.*, H and C) in inorganic substances.

Laboratory FTIR spectroscopy is used by geochemists to determine mineral structure (*e.g.*, Farmer 1974, van der Marel & Beutelspacher 1976), to quantify volatile element concentrations, isotopic substitutions and structural changes in natural and synthetic minerals, glasses and melts (*e.g.*, Farmer 1974, Rossman 1988a, McMillan & Wolf 1995, King *et al.* 2004), to examine the origin of color and properties of minerals (*e.g.*, Rossman 1988b, Clark 2004), to examine thermodynamic and transport properties of geologic materials (*e.g.*, Hofmeister 2004), to examine geologic materials *in situ* during heating, pressurization and/or deformation (*e.g.*, McMillan & Wolf 1995, Hofmeister 2004), and to examine geologic surfaces, such as those that have undergone chemical or biogenic processes (*e.g.*, Hirschmugl 2002a, b). Remote sensing researchers also use laboratory FTIR to calibrate the signal obtained from mineral mixtures (*e.g.*, web sites listed in Swayze 2004) so that remote sensing data can be "ground truthed". Data collected in the laboratory can also be used to produce spectra and/or algorithms that can then be applied to remote sensing or portable IR data (*e.g.*, Crowley 2004, Rivard *et al.* 2004, Swayze 2004).

To obtain the best possible IR spectra of samples it is necessary to choose the appropriate IR source, detection method and accessories. First, the analyst needs to determine the appropriate region of the infrared spectrum, in which the sample under investigation has diagnostic features. These regions are defined using wavelengths (λ) in microns (μm) or wavenumbers ($\tilde{\nu}$) in reciprocal centimeters (cm^{-1}), where $\lambda = 10^4 / \tilde{\nu}$. In terms of frequency, 1 cm^{-1} = 2.9979 x 10^{10} Hz ~30 GHz. Different users have defined the near-, mid- and far-IR regions

differently (Hirschmugl 2004), based on the practical limits of their instruments. To avoid confusion where specific spectral ranges are necessary we refer to the spectral ranges using both λ and ν.

The fundamental bands (Hirschmugl 2004) of relatively heavy metal ions, torsional modes, and other low-frequency excitations are typically located in the far-IR. Strong fundamental vibrations of the aluminosilicate framework of minerals and glasses, as well as the principal vibrational modes of most molecular species (*e.g.*, Si-O, C-O, S=O, and P-O) are located in the mid-IR. Moderately intense overtones (*i.e.*, $2\nu_{O-H}$, etc.) and combination bands (*e.g.*, $\nu_{HOH} + \nu_{O-H}$) due to even lighter groups (*e.g.*, H_2O, OH^-, CO_3^{2-}, SO_4^{2-}) are found in the mid- to near-IR. Also, electronic excitations (*e.g.*, Fe^{2+} transitions) are found in the near-IR. There are many compilations of typical IR absorbance regions for geologic materials and these are listed in the references in Clark (2004) and in McMillan & Hofmeister (1988).

Once the analyst has decided on the IR range of interest they need to decide on whether the sample can be analyzed in an atmospheric environment, whether there are restrictions on the sample type (*e.g.*, size, chemical and thermal characteristics), and how they wish to prepare their sample. It is also necessary to choose an optimal infrared source, interferometer unit, sample chamber, sample geometry and detector (Figs. 3-1 and 3-2). Finally, the methods for data acquisition and manipulation need to be defined.

The goal of the chapter is to provide the first-time analyst with a "shopping list" of mainstream commercial FTIR components and associated parts for analyzing geologic samples (Appendix 3-1). We provide a synopsis of sample preparation and analysis techniques, and methods that the analyst may choose to treat their data. Because this chapter constitutes an overview of a large number of topics we may have made inadequate generalizations in some instances; therefore, the interested analyst may want to consult other reviews and books on FTIR spectroscopy referenced below. We do not discuss dispersive IR instruments in any detail (*e.g.,* see Hadni 1967), and the chapter is not designed for experienced users or optical physicists/engineers.
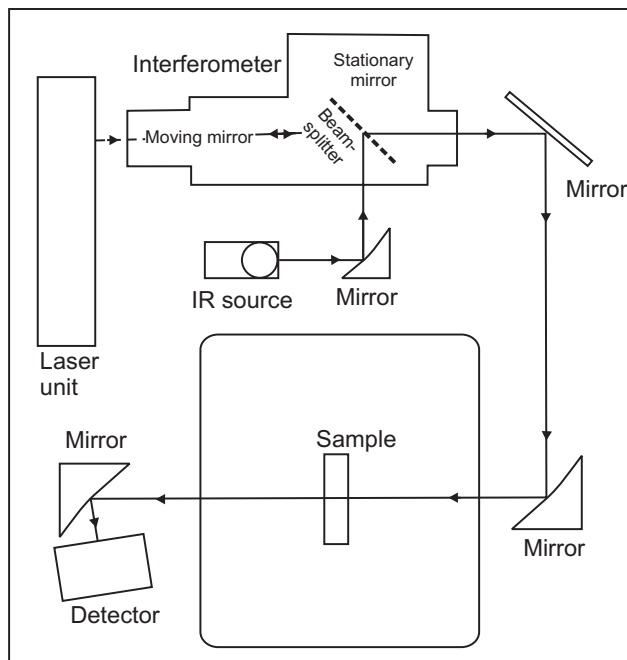

FIG. 3-1: IR spectrometer with the source, interferometer, sample, and detector. The interferometer and He-Ne laser systems are shown in detail in Figure 5a-b. The He-Ne laser is used as an internal reference and in some spectrometers it follows the same path as the IR beam beyond the interferometer unit in other spectrometers it is

detected separately. Diagram is modified from a Nicolet catalogue.

	Transmission	Reflection — Specular reflectance or bidirectional reflectance	Reflection — Attenuated total reflection	Reflection — Diffuse reflectance or biconical reflectance	Emission
Range	Remote sensing atmospheres/ hydrospheres	Laboratory techniques (10^{-9} – 10^{-1} g sample) — Laboratory microscope, mapping & polarization possible			Handheld devices (10^{-2}–10^{1} g sample) — Remote sensing planetary surfaces
Typical sample geometry	SOURCE → sample → DETECTOR. Transmission	SOURCE θ ⋮ θ DETECTOR, sample. Specular reflectance or bidirectional reflectance	SOURCE, DETECTOR, ATR crystal, sample, $n_c > n_s$. Attenuated total reflection	SOURCE, DETECTOR, sample. Diffuse reflectance or biconical reflectance	DETECTOR, sample, SOURCE=sample > 0 °K. Emission
Sample preparation & possible experiments	• powder, powder-carrier, low n polished wafer, films, liquids & gases • high T & P, kinetic & strain experiments	• high n polished solid, films • depth profiles possible if incident angle is varied • high T & P, kinetic & strain experiments possible	• powder, powder-carrier, films, solids, liquids • sample must not scratch/react with crystal & $n_c > n_s$ • depth profiles & strain experiments	• powder, powder-salt mix • high T & kinetic experiments	• powder, powder-salt mix
Quantification/Analysis procedure	Beer-Lambert law & characterize grainsize, density & thickness	Kramers-Kronig	Kramers-Kronig & characterize grainsize & density	Kubelka-Munk or Hapke & characterize grainsize, density & sample depth	Beer-Lambert law & characterize grainsize & density
Typical spectra	Absorbance vs Wavenumber (cm^{-1}); Transmission-%	Reflectance-% vs Wavenumber (cm^{-1}); Sigmoidal peak	log (1 / R) vs Wavenumber (cm^{-1})	Kubelka-Munk Units or Hapke apparent absorbance vs Wavenumber (cm^{-1})	Emissivity-% vs Wavenumber (cm^{-1})

FIG. 3-2: Summary flow chart showing which IR technique is the most appropriate for different sample types: transmission; reflectance including specular reflectance, attenuated total reflection (ATR), and diffuse

reflectance (DRIFTS), and emission.

INFRARED SOURCES
Thermal, unpolarized IR sources
Ideally, a thermal IR source is a black body radiator that is in thermal equilibrium and produces unpolarized (non-coherent), continuous radiation. The most common type of IR source used in laboratories is a filament held at high temperature. The overall efficiency or radiant flux, ϕ, (power in W) in any optical system from the source to the detector is described by:

$$\phi = L_{\tilde{v}}\, \tilde{G_v}\, (\Delta \tilde{v})\, \tau \qquad (1)$$

where $L_{\tilde{v}}$ is the spectral radiance of the source (power per area-solid angle-spectral bandwidth, W cm^{-2} sr^{-1}cm), G is the throughput (solid angle-area, sr cm^2), which depends on the spectrometer type, τ is the transmission of the system ($\tau = \phi / \phi_0$, W), and $\Delta \tilde{v}$ is the bandwidth of the instrument (in wavenumbers, cm^{-1}) (Schrader 1995). (Note: a modulation efficiency factor is also required in equation 1 if the beam travels through an interferometer, below).

The source produces emitted energy or a light quantum with energy hν, where, h is Planck's constant and ν is the frequency of the light. If the thermal source contains atoms or molecules in thermal equilibrium, then the spectral radiance, $L_{\tilde{v},T}$, can be modeled as an ideal black body (ε_λ=1.0) source using Planck's Law:

$$L_{\tilde{v},T} = \varepsilon_\lambda\, (2\, h\, c_0^2\, \tilde{v}^3) \, / \, (\exp[h\, c_0\, \tilde{v} \, / \, k\, T] - 1) \quad (2)$$

where, c_0 is the speed of light, T is temperature and k is a constant. Equation 2 can be used to determine the spectral radiance ($L_{\tilde{v},T}$) of a source for a range of temperatures and wavenumbers. Ideal blackbody curves for a range of temperatures are shown in Figure 3-3.

The type of filament used in the source depends on the infrared range of interest and can be determined from trade catalogs. Globar sources are versatile because they cover a wide energy (wavenumber) range, producing radiation in the far- to near-IR (~9600 - 50 cm^{-1}; ~1-200 μm). Quartz-halogen sources are used for near-visible IR applications (~27 000-2000 cm^{-1}; ~0.4-5 μm) and may have much higher spectral radiance due to their higher temperature, but their long wavelength limit

is imposed by the transmission through the "glass" envelope and they may drift in intensity. The spectral radiance for common (non-ideal) sources
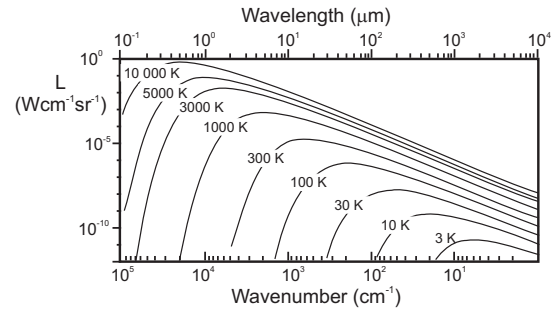

FIG. 3-3: A graphical representation of Planck's Law (equation 2) showing the spectral radiance, $L_{\tilde{v}}$ (W cm^{-2} sr^{-1}), of a black body radiator shown at a range of temperatures (3 - 10 000 K) versus wavenumber ($\tilde{v}$ in cm^{-1}) and wavelength (λ in μm). Note the distinctive "hump" shape in the IR region.

(Fig. 3-4a-c) deviate from the shape expected for an ideal black body source (Fig. 3-3) due to the non-unit emissivity of the source material.

Bright, pulsed, polarized, micro-IR sources
Accelerator-based and laser sources emit IR beams with high spectral radiance and high spatial resolution (<1 μm to 10's μm) with coherent or polarized radiation. Such sources may be used for a variety of applications (*e.g.*, commercial and military purposes, Jha 2000), but in this chapter we are most interested in their use for geologic specimens.

Bright, pulsed, polarized, micro-IR sources are ideal for small samples (*e.g.*, samples relevant to geomicrobiology, meteoritics, materials synthesized at high pressure), surface species (*e.g.*, weathering rinds), and samples with low energy, weak absorption signatures (such as films; for further applications see Hirschmugl 2002a, b). Another advantage is that these high spectral radiance sources may be pulsed to study *in situ* chemical reactions on mineral surfaces on rapid time-scales.

Accelerator-based sources have high spectral radiance IR radiation that is produced by accelerating charged particles (*e.g.*, electrons) in a magnetic field. In synchrotron-based IR, the electrons are accelerated around a storage ring and

may be pulsed at tens of picoseconds to nanoseconds.

In <u>free electron laser (FEL) sources</u>, the electrons are accelerated over short distances by a spatially varied magnetic field and then several
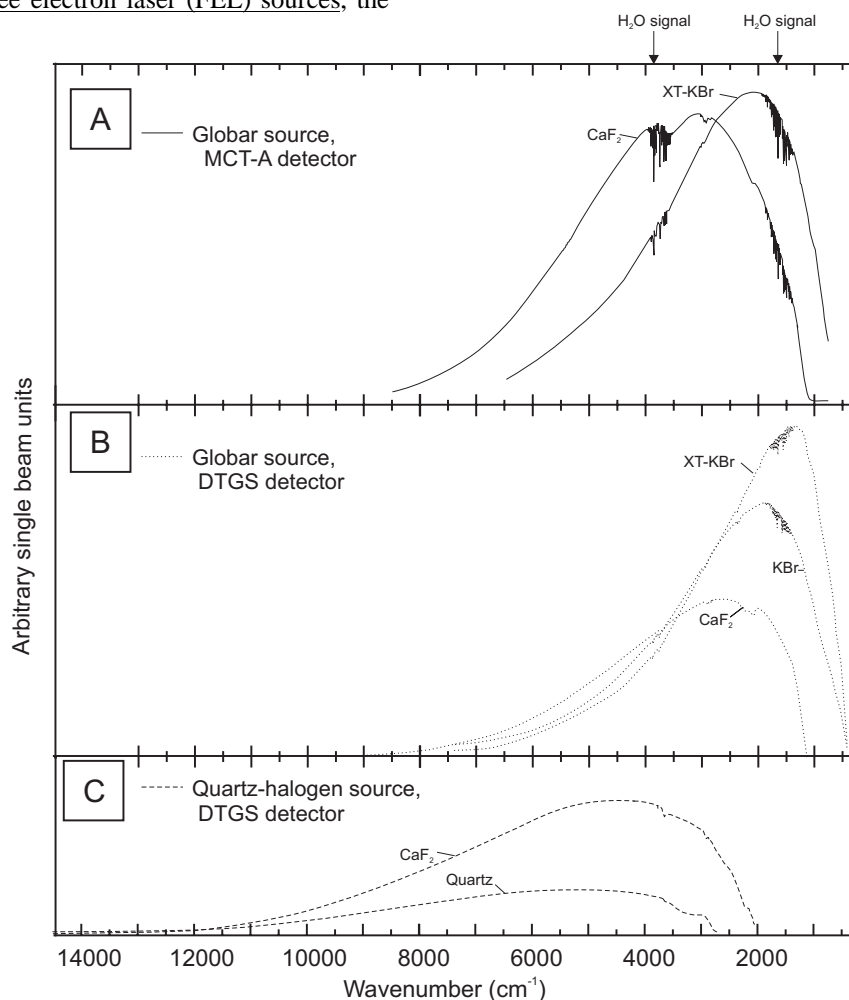

FIG. 3-4: A) Single beam spectrum collected with a Globar (Everglo) source, with an MCT-A detector and CaF_2 and XT-KBr beam splitters. B) Single beam spectrum collected with a Globar (Everglo) source, with a DTGS detector, and CaF_2, KBr and XT-KBr beam splitters. C) Single beam spectrum collected with a Quartz-Halogen source, with a DTGS detector and quartz and CaF_2 beam splitters. The H_2O bands were removed in the latter two spectra. The MCT-A detector spectra were collected at the University of Western Ontario and the DTGS spectra are redrawn from Nicolet technical notes (Kempfert *et al.* no date given; Leimer & Kempfert, no date given). The vertical scale is arbitrary because it depends on the spectrometer efficiency.

micro-beams are added to create the radiation used for analysis. These sources may be pulsed at 10^{-15} to 10^{-9} seconds. FELs provide high intensity beams, however intensities fluctuate therefore they are inherently not as stable as synchrotron sources.

THE MICHELSON INTERFEROMETER

Fourier transform infrared spectrometers use <u>interferometers</u> that allow a range of wavelengths to be produced near-simultaneously, thus decreasing the time required for analysis. This process is known as the <u>multiplex</u> or <u>Fellgett advantage</u>. Interferometric infrared spectrometers have high spectral radiance because all the IR radiation passes through, or is emitted or reflected from the sample and strikes the detector at once (the

Jacquinot advantage). In most commercial FTIR systems, the interferometer unit is a <u>Michelson interferometer</u> that includes a beam splitter, mirrors, and laser and in some cases an aperture (Fig. 3-5a, 3-5b).
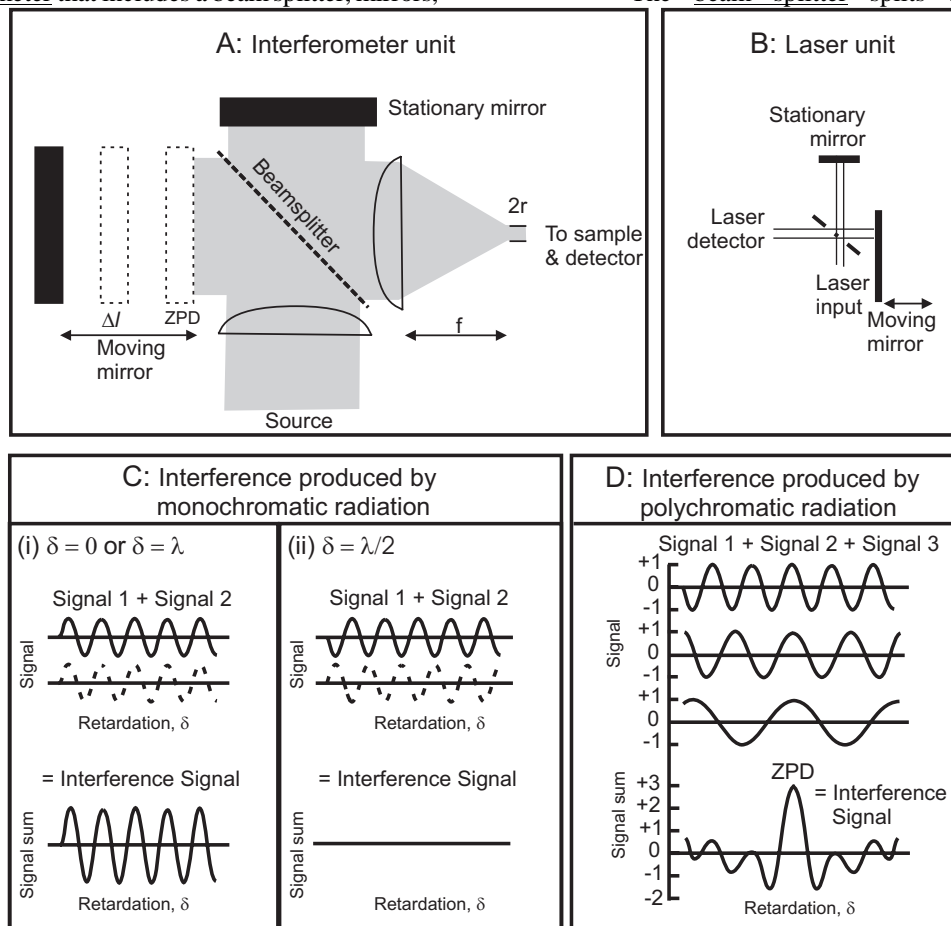
The <u>beam splitter</u> splits the source

FIG. 3-5: A) An interferometer unit with a moving mirror with displacement Δl and a Jacquinot aperture with a diameter 2r (modified from various sources). B) A laser unit showing how the laser also goes through a beamsplitter and is reflected from the moving and stationary mirrors. In some spectrometers, the laser follows the same path as the IR beam and in other spectrometers the laser follows a separate path. C) Schematic representation of the interference produced by adding monochromatic electromagnetic waves from the stationary mirror and movable mirror at different values of the optical path difference or retardation, δ. i) The optical path has a zero path difference (ZPD), $\delta = 0$ or λ causing the waves to interact constructively; ii) The optical path difference is one half of a wavelength, $\delta = \lambda/2$, causing the waves to interact destructively. Note that constructive interference occurs where the retardation is an integral number of wavelengths (modified after Griffiths & de Haseth, 1986). D) Schematic diagram showing how an interferogram is the sum of a series of electromagnetic waves of different wavelength (polychromatic radiation). Note that at ZPD, $\delta = 0$, the maximum signal is produced.

radiation with wavelength λ into two beams. After which, one beam is reflected by a stationary mirror with a fixed path length (represented by wavelength λ, in Fig. 3-5c) and the other beam is reflected by a moving mirror that moves over a distance Δl (Fig. 3-5a). Thus, the moving mirror reflects the second beam with a specific phase with respect to the first beam, and the phase changes as a function of mirror position. The difference in the path lengths is called the optical path difference or retardation (δ). The

mirror location at which both beams travel the same path length is known as the zero path difference (ZPD). The two beams are recombined at the beam splitter and then interfere constructively and destructively. A schematic diagram showing the interference is shown for a monochromatic wave in Fig. 3-5c. Constructive interference occurs where the retardation of the two mirrors is equal to $\delta = n\lambda$, where n is an integer. Destructive interference occurs where the retardation of the two mirrors is equal to $n\lambda/2$, where n is odd. For a monochromatic source one obtains a sinusoidal signal as a function of mirror position (Fig. 3-5c).

However, most sources are not monochromatic therefore, the signal must be viewed as a function of constructive and destructive interference from a polychromatic source (Fig. 3-5d). The signal obtained from the many wavelengths in the (polychromatic) source is a direct function of the optical path difference or retardation (δ):

$$I(\delta) = B(\tilde{v}) \cos 2 \pi \tilde{v} \delta \qquad (3)$$

where, $B(\tilde{v})$ is the intensity of single-beam spectrum, or the intensity of the source at wavenumber $\tilde{v}$, which is a function of the instrument δ (Griffiths & de Haseth 1986). Equation 3 defines an interferogram as a function of δ, which is the raw data that is collected and illustrated in Figure 3-6a. The interferogram is most intense at the ZPD where the greatest amount of constructive interference occurs and this area is known as the centerburst. The wings of the

interferogram are collected at larger optical path differences and with the spectral radiance and detectors used in most commercial FTIR instruments these have intensities close to zero (as discussed in the apodization section below). The interferogram is typically converted to the frequency domain using a Fourier Transform to produce an infrared spectrum of intensity versus energy in wavenumber or wavelength (Fig. 3-6b). The Fourier Transform process is discussed in more detail below.

Different beam splitters are sensitive over certain spectral ranges within the infrared region (Fig. 3-7). Common beam splitters are Mylar (far-IR), Ge-coated KBr or CaF_2 (mid-IR), and Si (near-IR). Care must be taken during collection of infrared spectra in the laboratory as different beam splitters materials used with the same source and detector will result in a different signal (Fig. 3-4a-c). For example, the lower limit of the spectral range decreases in λ (increases in $\tilde{v}$) with the following beam splitters: XT-KBr, KBr and CaF_2 with a Globar source and DTGS detector (Fig. 3-4b).

Some laboratory interferometers contain a reference He-Ne laser beam that is used to determine the position of the moving mirror and is

A: Interferogram of Earth's atmosphere with narrow centerburst

B: Single beam spectrum of Earth's atmosphere also known as the "background"
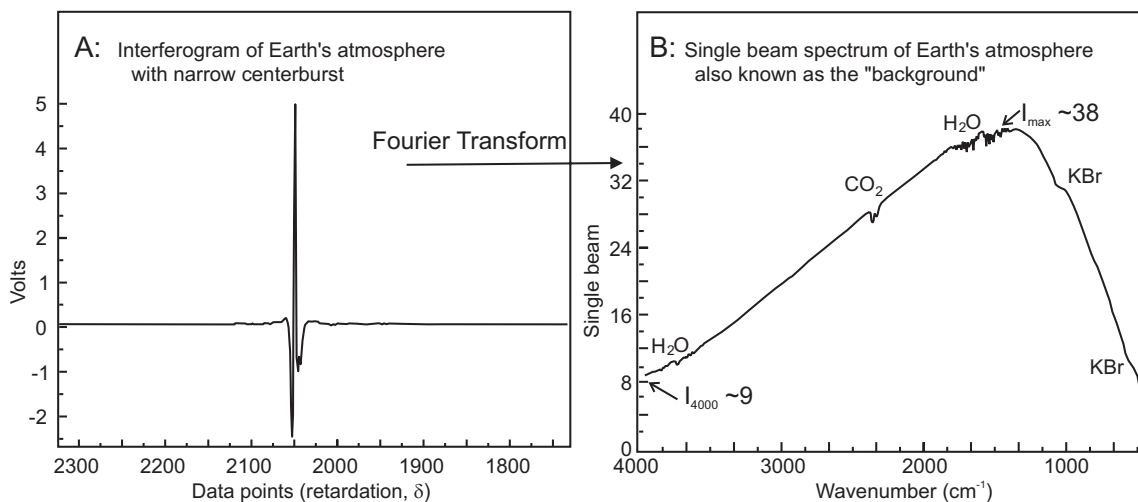
Fourier Transform

FIG. 3-6: A) Typical interferogram of Earth's atmosphere collected using transmission mode on an IR bench with a KBr beam splitter, Globar source and DTGS detector. There is no sample in the path of the IR beam, so this is a typical <u>background interferogram</u>. The interferogram is generally recorded as voltage versus optical path distance units; see text. B) Typical background spectrum of the interferogram after Fourier-transformation with a Happ-Genzel apodization function. Atmospheric bands (CO_2 and H_2O) and window bands (KBr) are shown. Also, the measurements that can be made to monitor instrument performance (I_{max} and I_{4000}) are shown, as discussed in Appendix 3-2.
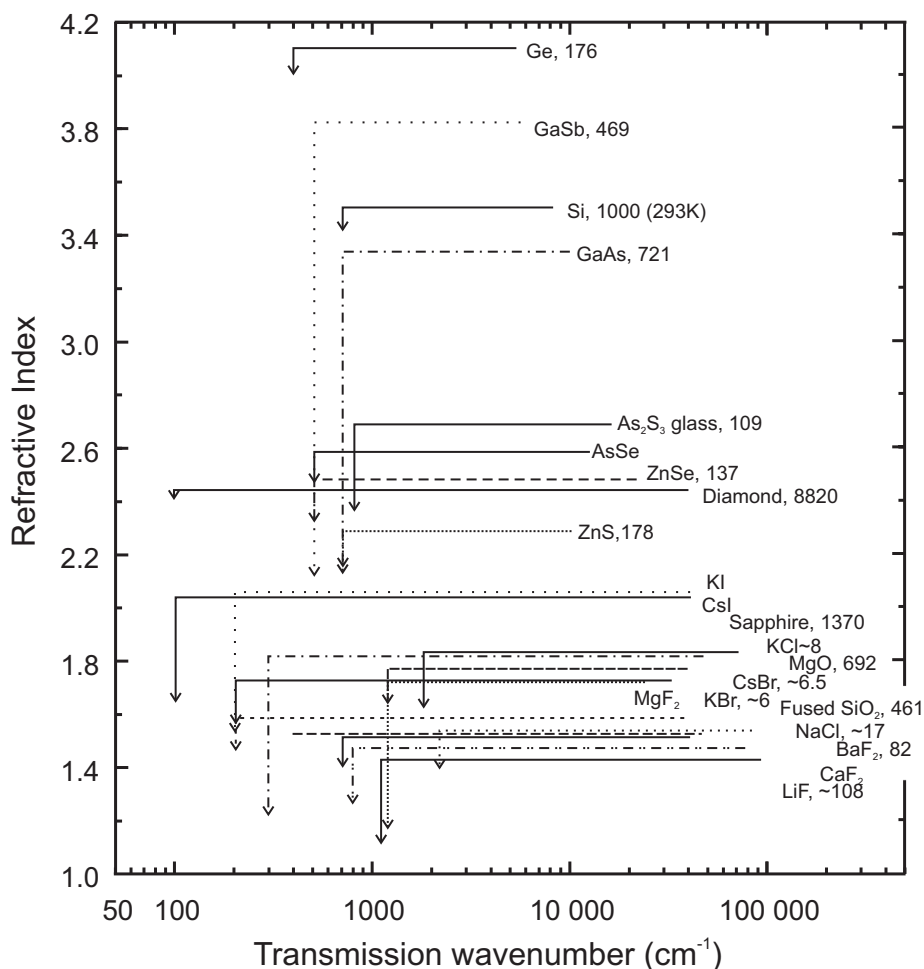

FIG. 3-7: Spectral ranges and refractive indices for different beam splitter and window types. The figure was constructed using data compiled in Wolfe & Zissis (1985). Note, that the refractive index actually shows a complex curved response, but this is not shown for the purposes of clarity; instead, the refractive index response is shown as a range indicated by the vertical arrow. Samples with high refractive index are used to refract the IR beam (e.g., Ge), whereas those with a low refractive index are used as "IR transparent" windows. The transmission range is the workable range for that window. The Knoop hardness ($kgmm^{-2}$) is also given for most substances.

detected synchronously with data collection (Fig. 3-1, Fig. 3-5b). The laser also acts as an internal frequency standard, because it radiates at 15,798.637 cm^{-1} allowing the wavenumbers to be detected with a precision of 0.01 cm^{-1} or better.

DETECTORS

Detectors transform the input energy (*e.g.*,

64

thermal energy, light quanta) into an output such as an electrical current or potential that is then converted to a signal. Sensitivity is measured as the noise equivalent power (NEP) (Fig. 3-8 for a variety of detectors), however, since the sensitivity of a given spectrometer is generally a nonlinear function of the detector size, the field of view it observes, the bandwidth used, the spectral radiance etc., it is difficult to use NEP for comparative purposes. For this reason, sensitivity is commonly expressed as specific detectibility (D*, pronounced "dee star", in $cmHz^{1/2}W^{-1}$) (Fig. 3-8) and this value can be used to determine order or magnitude differences between detectors. The analyst should choose a detector that provides the best signal in the region of interest because detectors are the largest potential
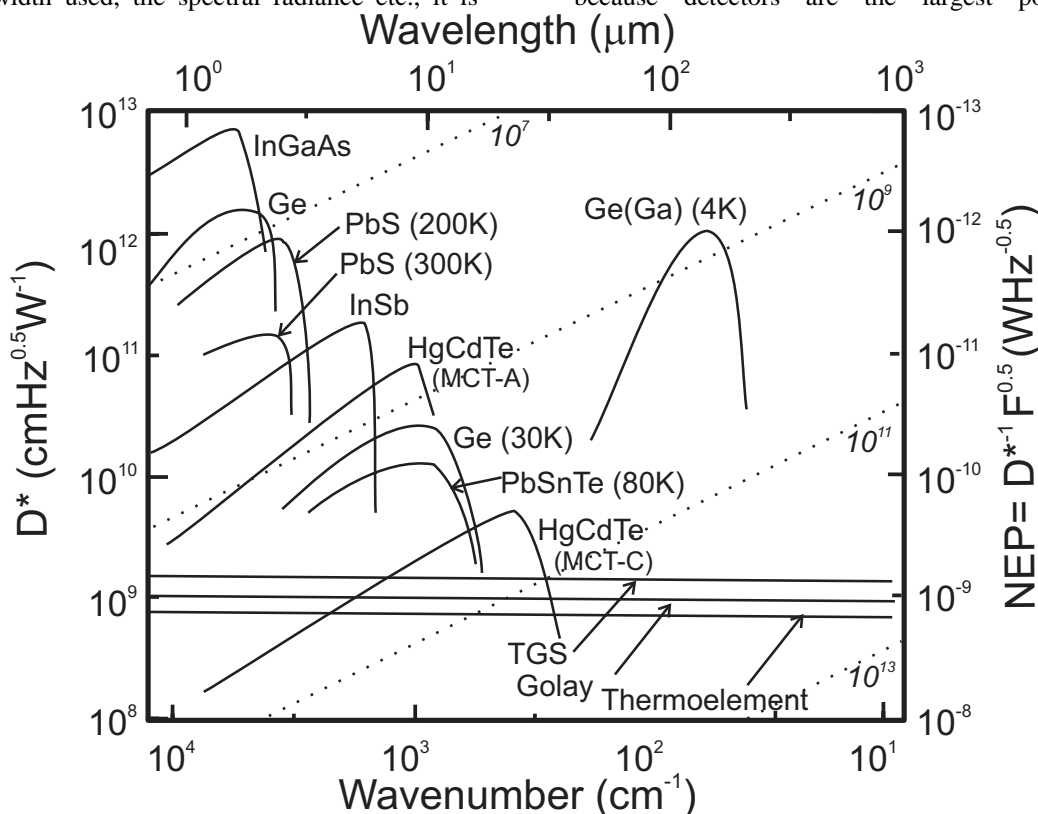

FIG. 3-8: Normalized detectivity, D*, for different detectors as a function of optical radiation (modified from Schrader, 1995). The NEP (noise equivalent power) is the incident radiant power resulting in a signal-to-noise ratio of 1 within a given bandwidth of 1 Hz and at a given wavelength. The numbers given in italics are the equivalent number of light quanta (hν).

contributors of noise in commercial Fourier Transform infrared spectrometers (Schrader 1995). There are many publications that discuss the engineering aspects of detectors (*e.g.*, Caniou 1999, Capper & Elliott 2001, Dereniak & Boreman 1996, Henini & Razeghi 2002, Jha 2000), and below we only summarize this field briefly. Some methods to minimize this noise are discussed below and in Appendix 3-2.

Thermal detectors convert thermal energy to electrical signal and include thermocouples, thermopiles, bolometers, pyroelectric detectors, and pneumatic and photoacoustic detectors. Pyroelectric detectors have a relatively uniform sensitivity throughout the entire spectral range (*e.g.*, Golay cells and thermoelements, Fig. 3-8) and they are relatively inexpensive and robust. The most common pyroelectric detectors are TGS (triglycerine sulfate) and DTGS (deuterated TGS) detectors. These detectors respond to temperature changes by changing their capacitance, which is measured as a voltage change. The major disadvantage of TGS and DTGS detectors is that they are less sensitive than other detector types. The other common types

of thermal detectors are bolometers that respond to temperature change by changing resistance, for example, Cu-, As-, In-, Ga- and/or Sb-doped Ge semiconductors, or doped Si semiconductors. Bolometers are sensitive detectors, but many models have the disadvantage of requiring liquid He and are relatively slow. Recently, stabilized micro-bolometers have been developed for use in spaceborne applications and these are less sensitive than the cryogenically-cooled bolometers.

Quantum detectors include In(Ga)As and InSb and liquid-nitrogen-cooled HgCdTe (MCT) detectors. These detectors operate when incoming IR radiation promotes electrons from the valence band to the conduction band where they can respond to an applied voltage. The major advantage of this detector type is much higher sensitivity (Fig. 3-8), that is necessary for micro-IR and directional hemispherical FTIR and they are particularly useful in dispersive or array grating IR systems used for high sensitivity measurements. The principal limitation of quantum detectors is narrower spectral range (Fig. 3-8) because the band gap (energy difference between the valence band and the conduction band) is controlled by either an impurity atom (*e.g.*, Pb and PbSe) or a mixture of semiconductors (*e.g.*, MCT detectors). For example, narrow band, high sensitivity MCT-A detectors commonly used for micro-FTIR are sensitive down to 700 cm^{-1} (~14.3 μm) and wide band MCT-B detectors are sensitive down to ~450 cm^{-1} (~22 μm) (Fig. 3-8). These detectors must be actively cooled to low temperatures typically using liquid nitrogen (in the case of laboratory and field instruments) or radiant cooling (in the case of spaceborne instruments). The other disadvantage of this detector type is that they have a maximum signal range upon which they become "saturated".

TYPES OF FTIR ANALYSES AND SAMPLE GEOMETRY

In this chapter we focus on three main types of FTIR analysis: transmission, reflectance and emission analysis. Figures 3-2, 3-9 and 3-10 summarize the typical sample geometries, sample preparation methods, applications of each technique and quantification procedures.

Transmission FTIR spectroscopy (T-FTIR) is typically carried out in the laboratory on solids, liquids and gases, but also may be performed in the atmosphere to determine gas concentrations. Transmission IR spectra may be presented as either transmission percent (Fig. 3-9a) or absorbance (Fig. 3-9b).

Reflectance FTIR spectroscopy (R-FTIR) can also be used in modes where there is reflection and/or scattering and/or attenuation of the IR beam with remote sensing, handheld and laboratory applications (Fig. 3-2). The many forms of R- FTIR spectroscopy are summarized in Figures 3-2 and 3-10. The simplest form of R-FTIR involves reflecting IR radiation from a flat surface where the angle of the incident IR light equals the angle of reflectance; this is known as specular reflectance or bidirectional reflectance (Figs. 3-2 and 3-10). T he type of reflectance method may be varied by changing the incident radiation (source collimation, Fig. 3-10) or detector collection mode (detector collimation, Fig. 3-10). Furthermore, reflectance
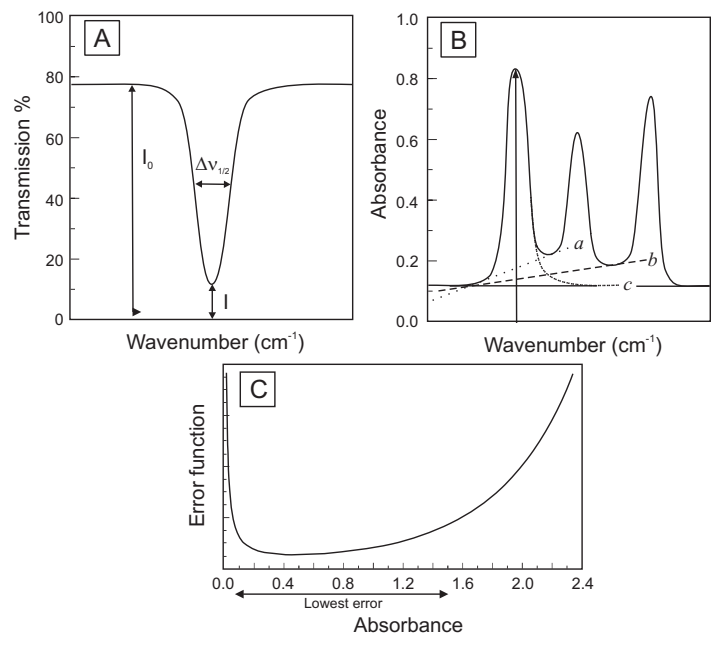
FIG. 3-9: A) Example spectra showing transmission % = T% = I/I_0, and indicating where measurements are taken. The full width at half height is also shown (FWHM or $\Delta\tilde{\nu}_{1/2}$); B) absorbance spectrum with a range of different possible baselines (a, b, c); C) error function of absorbance measurements modified from Schrader (1995).

Decreasing collimation of the DETECTOR

Collimated (directional)   Conical   Hemispherical

°θ

Sample

Decreasing collimation of the SOURCE

Collimated (directional)

θ°

Sample

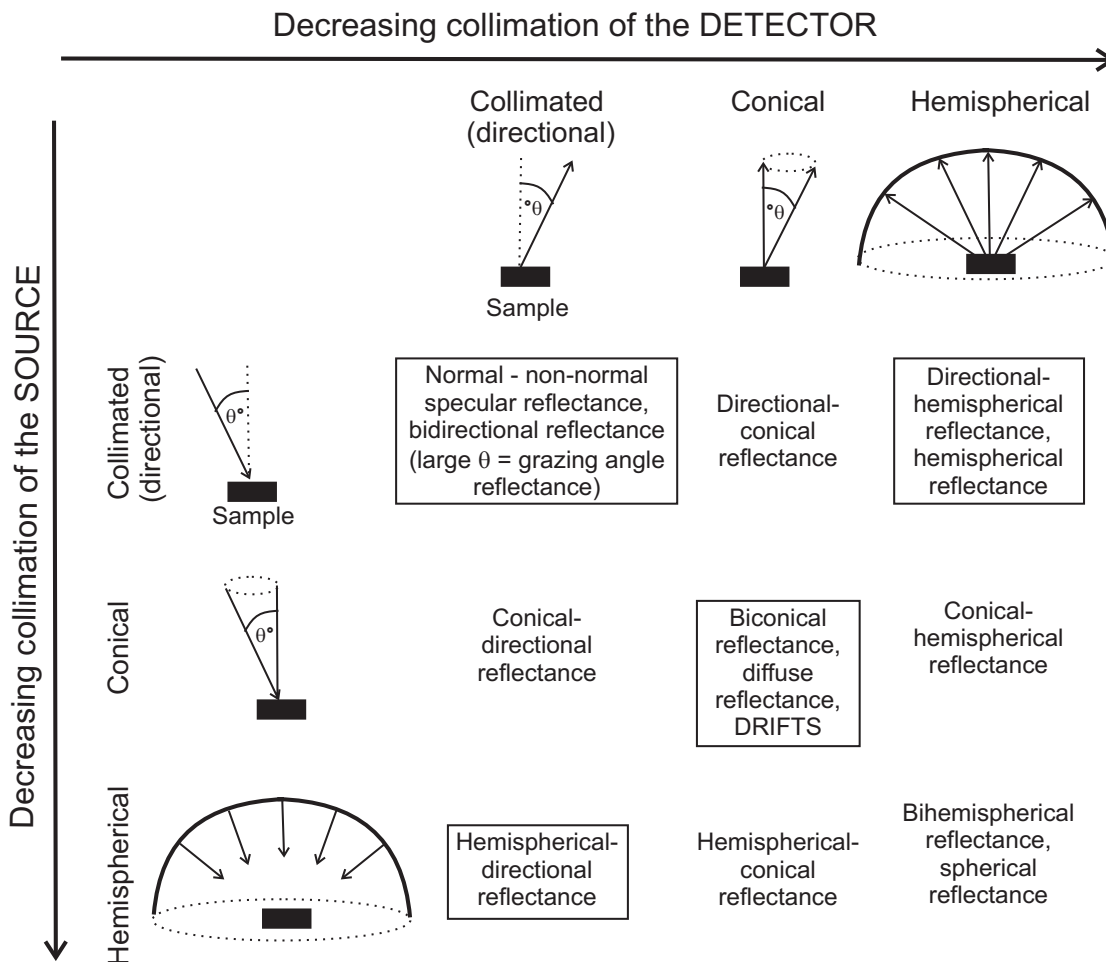|	Collimated (directional)	Conical	Hemispherical
Collimated (directional)	Normal - non-normal specular reflectance, bidirectional reflectance (large θ = grazing angle reflectance)	Directional-conical reflectance	Directional-hemispherical reflectance, hemispherical reflectance
Conical	Conical-directional reflectance	Biconical reflectance, diffuse reflectance, DRIFTS	Conical-hemispherical reflectance
Hemispherical	Hemispherical-directional reflectance	Hemispherical-conical reflectance	Bihemispherical reflectance, spherical reflectance

FIG. 3-10: Types of reflectance IR spectroscopy, defined based on the collimation of the detector (x-direction) and the collimation of the source (y-direction), modified after Hapke (1993). The methods outlined in boxes are discussed in the text.

spectra may be collected using a crystal with a moderate refractive index that attenuates the IR radiation (Fig. 3-7). Some reflectance peaks are "derivative shaped" (Fig. 3-2) and require treatment via Kramers-Kronig, Kubelka-Munk or Hapke algorithms (below, Fig. 3-2).

Emission FTIR spectroscopy (ε-FTIR) is primarily used in remote sensing (see review in Clark 2004) and emission spectra are reported as emissivity (Fig. 3-2). Emission IR spectra are commonly presented relative to the emissivity from a black body radiator (below).

The typical set-up, preparation, sample quantification and spectral output for each type of IR analysis are summarized in Figure 3-2. Both transmission and reflectance IR may be used in the laboratory with accessories such as a polarizer, microscope, microscope with a mapping stage, high temperature and/or high pressure/deformation cells, micro-ATR, and micro-grazing angle reflectance (Fig. 3-2). The general principles of micro-analysis are identical to bulk analysis, with the main differences being that a smaller sample may be analyzed, detectors with high detectibility are required (*e.g.*, MCT-A, Fig. 3-8) and the sample geometry is slightly different (see Fig. 4-7 in King *et al.* 2004).

In the following sections we discuss specific sample preparation techniques for the three FTIR analysis types, variables/media that may affect analysis, and data treatment. We then return to each of the three techniques, transmission, reflectance

(including specular reflectance and attenuated total reflection) and emission spectroscopy. We discuss the theoretical basis of each and discuss laboratory approaches. Remote sensing applications of IR are covered in more detail in other chapters of this volume. Other types of IR spectroscopy are discussed elsewhere, for example, photoacoustic spectroscopy (Michaelian 2003), polarization modulation FTIR spectroscopy (*e.g.*, Nafie, 1988), and synchrotron FTIR spectroscopy (Hirschmugl 2002b).

SAMPLE PREPARATION
Single crystals and polarization in solids

Infrared absorbance may be affected by bonds in a substance that are organized crystallographically (Fig. 3-11). Specifically, anisotropic materials have variations in both the refractive index and polarization ability, which depend on the crystallographic orientation. Thus, to obtain quantitative data on single crystals or information about the crystal geometry, it is necessary to use polarized IR radiation oriented to a crystal's refractive index axis (*e.g.*, to determine the H content in minerals, Rossman 1988a, or the optical constants of minerals, Wenrich & Christensen 1996). Uniaxial crystals (trigonal, tetragonal and hexagonal crystals) have rotational symmetry of their refractive index and polarizability around at least one symmetry axis. Biaxial crystals (orthorhombic, triclinic and monoclinic) have variable axis positions. Isotropic crystals and amorphous solids do not require orientation or polarized IR analysis. Crystallographically-oriented single crystals are tedious to prepare and the methods to do so include examining the optical properties of polished single crystals using a microscope and goniometer or spindle stage, or using micro-X-ray diffraction.

It is also possible to carry out IR absorption measurements directly on thin films using techniques such as grazing angle IR spectroscopy or synchrotron radiation (*e.g.*, Hirschmugl 2002a). In the case of crystalline minerals and amorphous substances, films that are only a few μm thick can be prepared using various techniques such as vapor deposition or melting (*e.g.*, King *et al.* 2004) or using a diamond anvil cell (Hofmeister 2004). However, if the samples are single crystals it is desirable that film samples
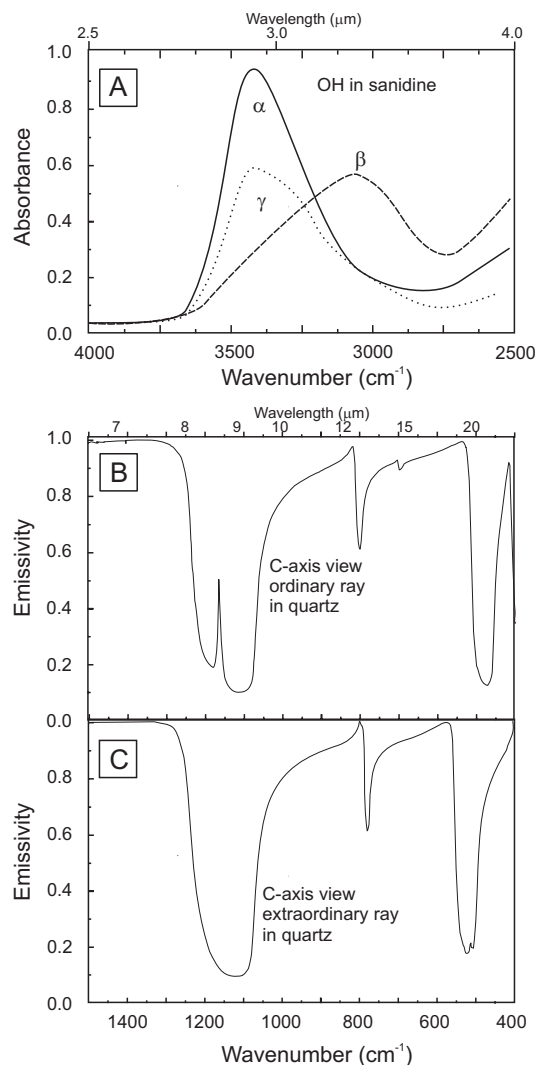

FIG. 3-11: A) Polarization effects in transmission IR spectroscopy of OH bands in 5.0 mm thick sanidine from the Eifel region, Germany, at different crystallographic orientations (redrawn from Hofmeister & Rossman, 1985). B) Polarization effects in emission IR spectra of quartz oriented to the ordinary ray versus C) oriented to the extraordinary ray (redrawn from Wenrich & Christensen, 1996).

should be oriented crystallographically, which is challenging in many cases.

Powders in transmission IR spectroscopy

To avoid polarization effects in transmission IR spectroscopy, non-cubic crystals are generally ground to a fine powder. Fine-grained

powders are prepared using mechanical vibrators, or mills, or with a mortar and pestle. Generally, samples are ground under acetone or ethanol to avoid damaging crystals or absorbing water during the grinding process. For nominally anhydrous minerals interaction of the sample with water is a particular problem (*e.g.*, Keppler & Rauch 2000).

For transmission analysis, the powder must have a random orientation and this is achieved by making a pellet or by supporting the sample on a window. In either method, the sample may be mixed with an IR transmissive salt or a "carrier" such as a mulling agent (*e.g.*, Nujol™ or Fluorolube™ or petroleum jelly) or a solution (*e.g.*, water, isopropanol or amylacetate etc.). In some cases it is advantageous to prepare a sample in more than one type of carrier in order to obtain spectra over a wide spectral range without signatures from the carrier.

Pellets have been one of the most common sample preparation methods. Typically, this approach entails lightly mixing ~100-300 mg dried KBr (400ºC, 6 hours) and ~0.7-2 mg of dried ground minerals and then placing the samples in a pre-heated 13 mm die (100ºC, ~20 mins) under a heat lamp. The material is pressed in a cylindrical die under a vacuum for 2-5 minutes at ~10 000 kg/cm^2 to produce a transparent sample disc. If, the disc appears "cloudy" this is likely due to water incorporated in the salt carrier and it may not be possible to properly interpret the 3000-3600 cm^{-1} (~3.3-2.8 µm) region (O-H stretching) and ~1610-1640 cm^{-1} (~6.1-6.2 µm) range (H-O-H bending) of the sample.

Scattering may occur as both surface scattering (off the sample surface) and volume scattering (where the radiation enters and exits the sample), dependent on the absorption coefficient and particle size (*e.g.*, Vincent & Hunt 1968, Ramsey & Christensen 1998, Hapke 1981). To avoid scattering problems in transmission analysis the powder must have a grainsize *smaller* than the wavelength of the radiation. It is possible to theoretically approximate this using Rayleigh's equation:

$$I_s = \left\{ I_0 \left(n_1 - n_2 \right)^2 * (1 + \cos^2 \theta * \pi^2 N V^2 \right\} / \left(n_2^2 r^2 \lambda^4 \right) \quad (4)$$

where I_s = intensity of scattered rays, I_0 = intensity of incident rays, n_1 = refractive index of the scattering particles, n_2 = refractive index of the embedding medium, V = volume of each scattering particle, N = number of scattering particles, λ = wavelength of the scattered radiation, θ = scattering angle, r = distance from the sample to the detector. The principal factors controlling scattering are therefore the particle radius (V term) and the region of the IR under study (λ). In practice, Rayleigh's equation (equation 4) is only valid when the grain is much smaller than the wavelength and so generally the grainsize should be much less than λ/π.

The infrared absorption process involves an interaction between the fluctuating electric vector of the incident IR light beam, E(t), and an oscillating dipole moment created within the sample by the vibration, $\Delta\mu$(t). Minerals and silicate glasses are often strongly ionic materials, and their stretching and bending vibrations can be associated with large values of $\Delta\mu$(t), and thus give rise to very strong infrared absorption. For this reason, passage of an IR beam through samples any thicker than a few µm or tens of µm will result in complete attenuation of the beam in the vicinity of the absorption frequency. This is why the powder transmission method described above is so popular: it permits the preparation of 1-5 µm particles that are then suspended in an IR transparent medium and held within the beam, to permit study of the strongly IR-active vibrations by transmission spectroscopy. However, there are pitfalls associated with interpretation of the results obtained by powder transmission experiments that are described below (McMillan 1984, McMillan & Hofmeister 1988).

The problems arise from the fact that the data are obtained from passage of an IR beam through an aggregate of solid particles that can reflect the beam from their surfaces as well as interfere with it because of the particle size distribution and the average interparticle spacing. Silicate minerals and glasses are largely ionic solids, and the collective solid-state vibrations are separated into "transverse" and "longitudinal" optic (TO and LO) modes, according to their direction of propagation relative to the direction of passage of light through the sample. The LO modes occur at a frequency that is higher than that of the corresponding TO vibrations, by a factor that is determined by the "ionicity" or the magnitude of the dipole moment change ($\Delta\mu$) associated with the vibration; this can cause TO-LO separation of several tens up to hundreds of cm^{-1} (McMillan 1984, McMillan & Hofmeister 1988). Only TO

modes are observed in "pure" absorption experiments, but LO contributions appear in reflectance measurements (below). The "powder transmission" data can contain contributions from both TO and LO features, due to the simultaneous existence of transmission paths through the particles and multiple reflectance from their surfaces, and so the resulting spectra are often an unresolved (and irresolvable) mixture due to IR absorption/ reflectance effects. The result can include (a) shifts in measured transmission minima to higher wavenumber (lower wavelength) than the expected IR absorption (TO) frequencies, (b) broadening and distortion of transmission band shapes from those expected from either pure absorption or reflectance studies, (c) appearance of additional features in the spectra that can be ascribed to purely surface modes of the particles, and (d) interference fringing or channeling (below) due to interference and diffraction of IR radiation related to the particle size distribution and the average interparticle spacing (Decius & Hexter 1977, McMillan 1984, McMillan & Hofmeister 1988).

Although useful results can be obtained using the IR powder transmission method, and many data are present within the literature concerning geologically-important minerals and glasses, these should be treated and evaluated with care in the light of the concerns and considerations above.

Powders in reflectance and emission IR spectroscopy

Powders are a convenient way to prepare samples for diffuse reflectance and emission spectroscopy, where scattering is advantageous. In contrast to transmission IR techniques, in reflectance and emission IR, powders are generally LARGER than the wavelength of light. The effect of the powder grainsize on reflectance and emittance has been described in detail elsewhere (*e.g.*, Clark 2004, Hapke 1993, Moersch & Christensen 1995, Salisbury & Wald 1992, Wenrich & Christensen 1996).

In emission spectroscopy, fine-grained powders result in smaller optical path lengths and diffraction effects. Typically, particles on the order of 100-500 μm are used to avoid both the particle size effects and obtain the random orientation. For emission (and by extension, remote sensing), particle size is problematic where it is less than approximately 10x the wavelength (~100 μm). This

is due to the smaller optical path length the photon travels through the particles and the non-linear interaction of that photon as it reflects with multiple particles (Hunt 1976, Moersch & Christensen 1995).

With decreasing particle size, significant changes in the shape of the spectral features become an issue. The behavior of these changes is ultimately related to the variation of the optical constants for each mineral, therefore, the changes vary as a function of wavelength. These constants are discussed in detail for quartz (Moersch & Christensen 1995). The change in band shape and depth can be monitored in three main spectral regions: the reststrahlen bands, the intraband regions and the Christensen frequency (Fig. 3-12).

First, at the reststrahlen bands, which dominate vibrational spectra at large grain sizes, the mineral has a high absorption coefficient. With decreasing particle size, the positions of the reststrahlen bands remain nearly constant, however, the grains with a much larger surface area increase the potential of multiple reflections and hence the subsequent amount of energy returned to the detector (Lyon 1965, Salisbury & Wald 1992, Moersch & Christensen 1995). In an emissivity spectrum, this scatter of emitted energy produces the linear effect of reducing the spectral contrast of the reststrahlen features (*i.e.*, the emissivity is higher, Fig. 3-12).

Second, in spectral regions where the mineral is weakly absorbing, known as the intraband regions or transparency features, volume transmission through the grains dominates. As particle size is decreased, more surface interfaces are created and the potential for energy to escape the surface is reduced (Lyon 1964, Salisbury & Wald 1992, Moersch & Christensen 1995). In these intraband regions, emissivity decreases with grain size giving rise to new apparent absorption bands, which continue to increase in intensity (*i.e.*, the emissivity is lower, Fig. 3-12).

The third primary behavior observed in the spectra of particulates occurs in the region where the index of refraction (n) is near-unity and the absorption coefficient increases sharply. At these wavelengths, very little energy is scattered (Moersch & Christensen 1995) so that the reflectance becomes very small and the emissivity approaches one. Known as the Christiansen frequency, these regions remain unaffected by changes

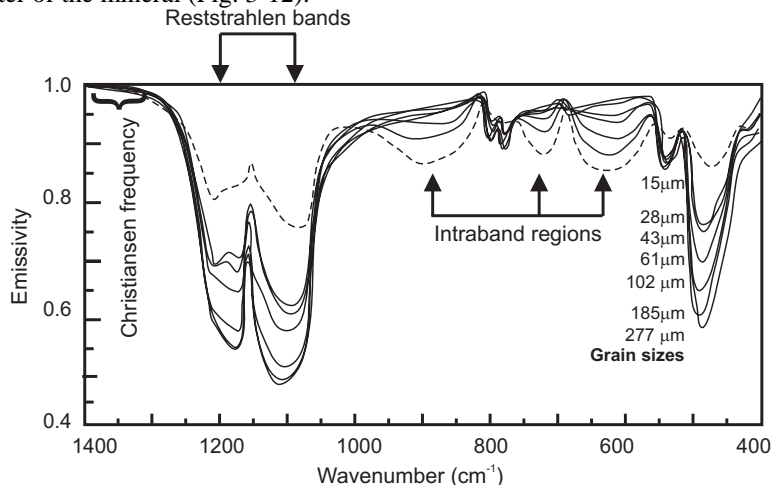in the grain diameter of the mineral (Fig. 3-12).

FIG. 3-12: Emissivity measurements for quartz grains of different sizes (15-277 µm). In the restrahlen band regions, the emissivity generally decreases with increasing grain size. The emission decreases in intensity with decreasing grain size in the intraband regions. The emission at all particle sizes is uniformly high at the Christensen frequency (~1300-1400 cm^{-1}). Diagram is modified from Moersch & Christensen (1995) and some spectral resolution has been lost in the modification process.

Preparation of solids for micro-FTIR

Solids may be prepared in the same manner for micro-FTIR analyses as bulk analyses, but the advantage is that a smaller area may be analyzed using a microscope attachment (see Figure 3-2). For instance, instead of preparing a several milligram crystal, an area on a sample ~100 µm across may be easily analyzed with a high SNR. Another advantage of micro-FTIR is that it is possible to compress milligram amounts of powders in a diamond anvil cell and analyze a thin film, in some cases at high temperature and/or pressure (*e.g.*, Hofmeister 2004) or at the same time as deformation. The spatial resolution in micro-FTIR analysis is affected by the limit of diffraction for the system and the SNR. Synchrotron micro-FTIR is particularly advantageous for high spatial resolution micro-FTIR due to the high intensity of the source, resulting in a high SNR.

MEDIA THAT MAY AFFECT SAMPLE MEASUREMENTS
Background and spectrometer contributions

The spectral radiance of a spectrometer system varies as a function of age and the component spectrometer parts (Fig. 3-1; IR emission intensity of the source as a function of wavelength, the optical transmission, the wavelength-dependent efficiency of the detector, the modulation efficiency of the interferometer, the solid angle viewed by the detector, and its responsivity etc.). Therefore, each analysis needs to be ratioed to the IR intensity incident on the sample (I_0) in order to examine the signal that is derived from the sample only (I_{trans}). The measurement of the IR intensity incident on the sample is known as the background, although technically this is a reference spectrum.

For transmission spectroscopy, the sample spectrum always contains a signal from the background (signal from the spectrometer without a sample present, *e.g.*, Fig. 3-6a). To find the signal derived only from the sample it is necessary to make a background measurement and ratio the sample + background measurement to the background. Ideally, both the background and the sample should be collected under the same conditions (*e.g.*, temperature, number of scans and purge conditions) and should be reproducible. For reflectance spectroscopy, the background is collected using a highly reflective, spectrally flat plate ($R_\lambda \sim 1.0$, $\varepsilon_\lambda \sim 0.0$) such as Au in the mid- to far-IR because it reflects near 100% of the IR radiation in this range. Commonly Ag is used for the visible-near-IR range; also polished Al, stainless steel and commercially available materials (*e.g.*, Halon and Spectralon) are

used for some applications (Clark 2004, Salisbury *et al.* 1991, Ruff *et al.* 1997). For emission spectroscopy, the background is collected as a spectrum of a near-ideal blackbody at one or more temperatures ($\varepsilon_\lambda \sim 1.0$, $R_\lambda \sim 0.0$, for emission), as described in more detail below.

Most laboratory-based spectrometers are set up to automatically subtract the background once it has been obtained (subtract for transmission or divide for reflectance and emission, Clark 2004) and so the user may never specifically use the interferogram. However, it should be noted that the interferogram is the raw data and that this information should be saved in cases where the background may vary.

In all types of IR measurements, the most likely bands to appear in the background spectrum are the IR-active gases in the atmosphere: CO_2 (2350, 667 cm^{-1}; 4.25, 15 µm) and H_2O (3900-3400, 1850-1350 cm^{-1}; 2.56-2.94, 5.4-7.4 µm). These bands will appear as positive or negative bands in the sample spectrum if the background and sample were not collected under the same purge conditions. Many laboratory infrared spectrometers are purged with dry nitrogen or dry, CO_2-scrubbed air to minimize atmospheric contributions.

In laboratory IR measurements, where a "carrier" has been used to support or dilute the sample, it is generally advantageous to take a spectrum of the carrier as a background. A background of liquid carriers is essential, however, it is not recommended to take the spectra of solid carriers such as KBr that are hygroscopic because the H_2O bands are difficult to duplicate (Smith 1996), even if the KBr has been heated. Other bands that may occur in samples are C-H stretches (2800-3200 cm^{-1}; 3.1-3.6 µm) due to fingerprints (Table 3-1).

TABLE 3-1 - SPECTRAL RANGE FOR TYPICAL BACKGROUND CONTRIBUTIONS

Species	Source	Wavenumber (cm^{-1}) *	Wavelength (µm)
CO_2 (g)	Atmospheric	~4870-5000 (s)	2.01, 2.06
		~6250 (w doublet)	~1.6
		2350 (vs- doublet)	~4.25
		667 (m)	15.0
H_2O (g)	Atmospheric	3900-3400 (vs)	2.6-2.9
		1850-1350 (s)	5.4-7.4
SO_2 (g)	Atmospheric, anthropogenic	1140-1080 (s)	8.8-9.3
O_3 (g)	Atmospheric troposphere, anthropogenic	~1042 (s)	~9.6
		~28 500 (vs)	~0.35
O_2 (g)	Atmospheric	~13 100 (s)	0.76
Si-O	Aerosol- soil	1110-1000 (s)	9.0-10.0
		805 (m)	12.4
		450 (m)	22.2
S-O in SO_4^{2-}	Aerosol- salt	1140-1080 (vs)	8.8-9.3
		680-610 (m)	14.7-16.4
C-O in CO_3^{2-}	Aerosol- salt	1510-1410 (vs)	6.6-7.10
		880-860 (m)	11.4-11.6
		710-750 (m)	14.1-13.3
P-O in PO_4^{3-}	Aerosol- salt, anthropogenic	1100-1000 (s)	9.1-10.0
		600-500	16.7-20.0
N-H	Biologic and anthropogenic	3500-3200	2.9-3.1
N-O in NO_3^- &	Biologic and anthropogenic	1400-1340 (vs)	7.1-7.5
N_2O		840-810 (m)	11.9-12.4
		720 (m)	13.9
C-H	CH_4, biologic and fingerprints	3200-2800 (s)	3.1-3.6
Si-CH$_3$	Si-based grease and oils	1270 (s)	7.9

Aerosol data from Berner & Berner (1996) and wavenumbers for compounds from Smith (1999) and Clark

(2004). * vs = very strong; s = strong; m = moderate.

In hand-held and remote-sensing IR, the atmospheric absorption bands (CO_2 and H_2O) contribute significant spectral features, in addition to those derived from other IR active gases such as O_3, SO_2 and CH_4. Tropospheric O_3 (~1040 cm^{-1}, 9.6 µm) is a factor for spaceborne measurements, whereas SO_2 is typically present near active volcanic sources and CH_4 is found in agricultural regions. In addition to the gases, aerosols and dust from marine, continental, biological and anthropogenic sources can contaminate the surface spectrum. However, these are in such low concentrations that they generally do not affect the IR spectrum, but they may be abundant locally. Infrared-active compounds in the atmosphere include sulfate salts derived from sea spray (*e.g.*, gypsum), aerosols derived from soils and salt pans (*e.g.*, gypsum, calcite, silicates, phosphates and nitrogen compounds), and, compounds derived from biological sources, biomass burning and industrial pollutions (phosphorous, nitrogen and sulfur compounds). The wavenumber and wavelength ranges for these possible background bands are given in Table 3-1.

Windows and carriers

Infrared windows can either be used to enclose a sample in a cell (*e.g.*, high-pressure, high-temperature or liquid cell) or as supports on which the sample is dispersed or flattened using a roller, or as a barrier from the environment through which the incoming IR radiation passes. Generally, windows are treated in the same way as an atmospheric background: a measurement is made of the "clean" window and then a measurement is made of the window plus sample and the window spectrum is subtracted/divided out.

Windows should not absorb IR radiation in the region of interest, should be hard enough to withstand scratches (particularly important for minerals), should not react with the sample or atmosphere and should have a relatively low refractive index. The refractive index affects whether the IR energy from the material will undergo total internal reflection (reflections off the crystal-air interface and the air-window interface). It is recommended that the absorbance measured for windows should be less than 1 to minimize problems with phase correction (Schrader 1995).

Figures 3-7 shows typical values for refractive index, transmission ranges and hardness for common window types. Further information may be obtained from IR manufacturers or in library reference collections (*e.g.*, Caniou 1999, Kokorina 1996, Wolfe & Zissis 1985).

VARIABLES DEFINED BY THE ANALYST
Spectral sampling and spectral resolution

The analyst must choose the sampling interval at which to resolve a spectral feature; this is commonly referred to as the spectral sampling and is defined as the sampling interval (number of data points) measured for a given frequency or wavelength change: $R = \tilde{v}/\Delta\tilde{v} = \lambda/\Delta\lambda$ (Fig. 3-13a, b). The sampling interval should be chose so that the peak and valley locations of the peak can be unambiguously defined; this is discussed in more detail in the section on "Apodization" below.

The theoretical upper limit of the resolving power R_0 for the sampling interval in a Fourier Transform infrared spectrometer is primarily determined by the path length of the moving mirror, Δl (Fig. 3-5a). For spectral sampling less than 4 cm^{-1} (4 nm when $\lambda = 10$ µm), an aperture is used to minimize non-parallel radiation that may reduce the contrast in the interferogram at high path differences. In this case, the spectral sampling depends on Δl in addition to the radius of the so-called Jacquinot stop aperture, r, and the focal length, f, of the entrance optics into the aperture (Fig. 3-5a).

Commonly spectral sampling is confused with spectral resolution (*sensuo stricto*), which is the ability to resolve a spectral feature and is defined as the minimum spectral separation required for discriminating two spectral features. Spectral resolution depends on the FWHM, wavelength location of band centers and sampling interval. Practically, the spectral resolution of a spectrometer should be determined for every machine as discussed in Appendix 3-2.

The detailed bandwidth (and band shape) of the spectral feature is a function of the mean lifetime for a molecule to relax from the vibrational level that was achieved where the molecule was excited by the IR radiation (Hirschmugl 2004). For vibrational processes the bandwidth (also called bandpass) can be measured using the full-width at

half-maximum of the band (FWHM, $\Delta\tilde{v}_{1/2}$ or $\Delta\lambda_{1/2}$, Fig. 3-9a).
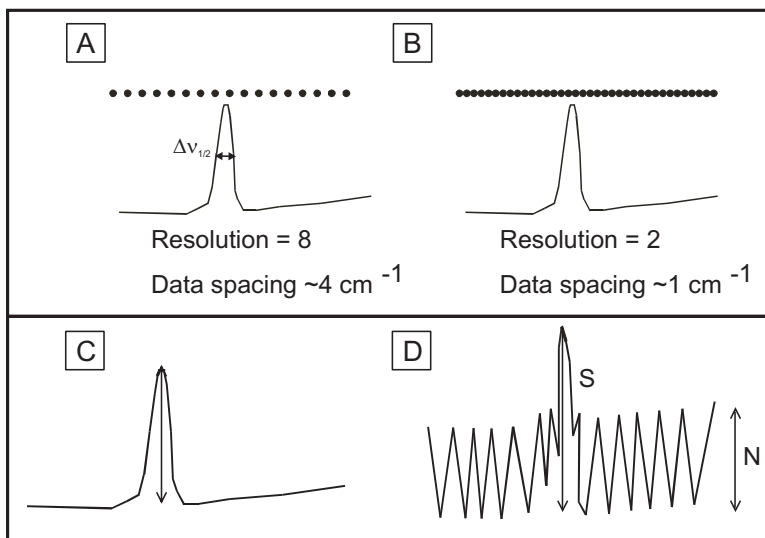

FIG. 3-13: A) and B) are schematic diagrams showing spectral resolution at different values and the effect on data spacing. The full-width at half maximum (FWHM or $\Delta v_{1/2}$) is also shown. C) Schematic diagrams illustrating the concept of good signal-to-noise-ratio (SNR). D) Schematic diagram illustrating a large amount of noise (SNR = S / 1σ(N)).

Signal-to-noise ratio (SNR)

Noise is inevitable in any real system and the goal of the analyst is to reduce the noise relative to the signal. The source carries noise owing to random photons and the detector has thermodynamic noise in interaction with these photons. In addition, unwanted noise may be produced by environmental factors (*e.g.*, temperature fluctuations, electrical interference, external vibrations, and radiation noise), which can be minimized by placing the spectrometer in an appropriate location (see Appendix 3-1). Increasing the measurement time or modulation can reduce other types of noise, such as white noise (random errors inherent in the analysis), fluctuations and drift (*e.g.* electronic drift or non-linear interference caused by the composition of the matrix in which the element to be analyzed resides). For further details regarding noise the reader is referred to other publications (*e.g.*, Dereniak & Boreman 1996).

The signal-to-noise ratio (SNR) is measured by the sample absorbance (S) over one standard deviation of the signal at a baseline point nearby in the spectrum (N) (compare Fig. 3-13c with Fig. 3-13d). If the signal from the band and noise are interdependent, then one approach is to obtain a statistically significant number of sample spectra, and directly measure the statistics of the variation of the signal of interest (*e.g.* the absorbance). Further methods to distinguish a band, independent of noise, are discussed in detail in Swayze *et al.* (2003).

For a interferometer-style spectrometer, the SNR is proportional to the number of scans or number of times that spectra are collected from the same sample and then co-added to produce the final spectra. The SNR is related to the number of scans following the relation: $SNR \propto (t/t_A)^{1/2}$, where t = the total measurement time and t_A = the time to measure one channel (*e.g.*, Griffiths & de Haseth 1986). The effect of increasing scan time is shown in Table 3-2.

Samples collected at high spectral resolution (closer data spacing) are inherently noisier than low spectral resolution data because the former are measured with large optical path differ-

TABLE 3-2. RELATIONSHIP BETWEEN THE NUMBER OF SCANS AND SNR

# Scans	SNR improvement relative to 1 scan
1	-
4	2

16	4
64	8
256	16
1024	32

ences: SNR $\propto$ spectral resolution. High spectral resolution data collected with a Jacquinot stop aperture are noisier because there is less signal transmission.

If sample noise is problematic for long collection times (with the co-addition of multiple scans) it is possible that environmental factors and instrument drift may be affecting the noise. It is recommended to increase the sample quality, use lower spectral resolution, or use a different sampling technique. Another approach is to smooth the spectra (Hannah 1988, Hawthorne & Waychunas 1989), using a technique such as a running average (*e.g.*, Savitzky & Golay procedure), but this reduces the spectral resolution.

Instrument gain

The analyst is able to change the instrument gain (amplification) to obtain a larger signal from otherwise low amplitude wavelength regions. Figure 3-14 (a, b) shows that increasing the gain amplification increases the amplitude of the interferogram (I_0) for a symmetric wavelength difference around the ZPD centerburst ($I_{with\ gain}$). Increasing the gain in this wavelength region has the advantage of increasing the dynamic range of the analog-to-digital converter, however, it has the disadvantage of increasing the noise in the centerburst region.

FOURIER TRANSFORMATION

As shown, in equation 3, the interferogram is a function of the retardation (δ), or mirror velocity (v) and time (t) (Griffiths & de Haseth 1986). This equation has a cosine Fourier transform relation between intensity of the beam at the detector, $I(\delta)$, and intensity of the single-beam spectral intensity, $B(\tilde{v})$. To retrieve the intensity data from the single-beam spectrum it is necessary to perform a Fourier Transform. A Fourier Transform of a cosine wave from a monochromatic source would result in a single peak (Figure 3-15a). A Fourier transform of a complicated wave, such as that in a standard polychromatic source results in many peaks (*e.g.*, Fig. 3-15b-d).

Apodization

Interferograms are not collected over a distance from minus to plus infinity, but instead the data is truncated by the limits of the moving mirror (the limits are ZPD and ZPD + Δl). Because the
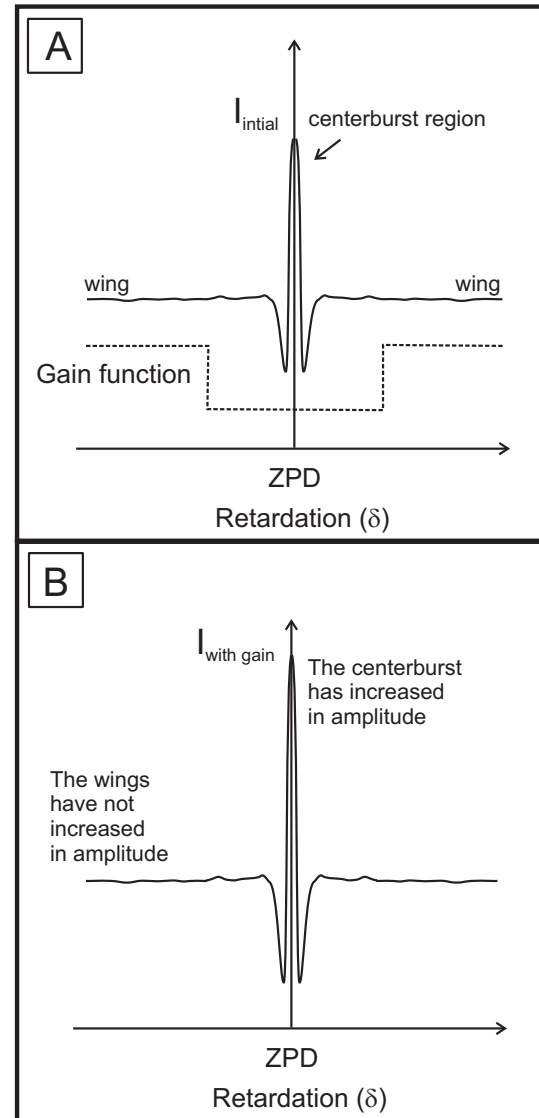

FIG. 3-14: The effect of a gain-ranging amplifier on the interferogram (from Griffiths and de Haseth, 1986). A) The original interferogram and gain function. B) The interferogram after the gain function has been applied. Note that the signal is only amplified in the area near the centerburst.

data are truncated the spectrum has discontinuities (analogous with viewing data through a limited window with sharp edges) that are problematic for

the Fourier transform procedure. Apodization refers to numerically altering the interferogram by multiplying it by a weighting function that modifies its intensity such that it approaches zero at its limits, thus, the data has "softer edges" and there are less
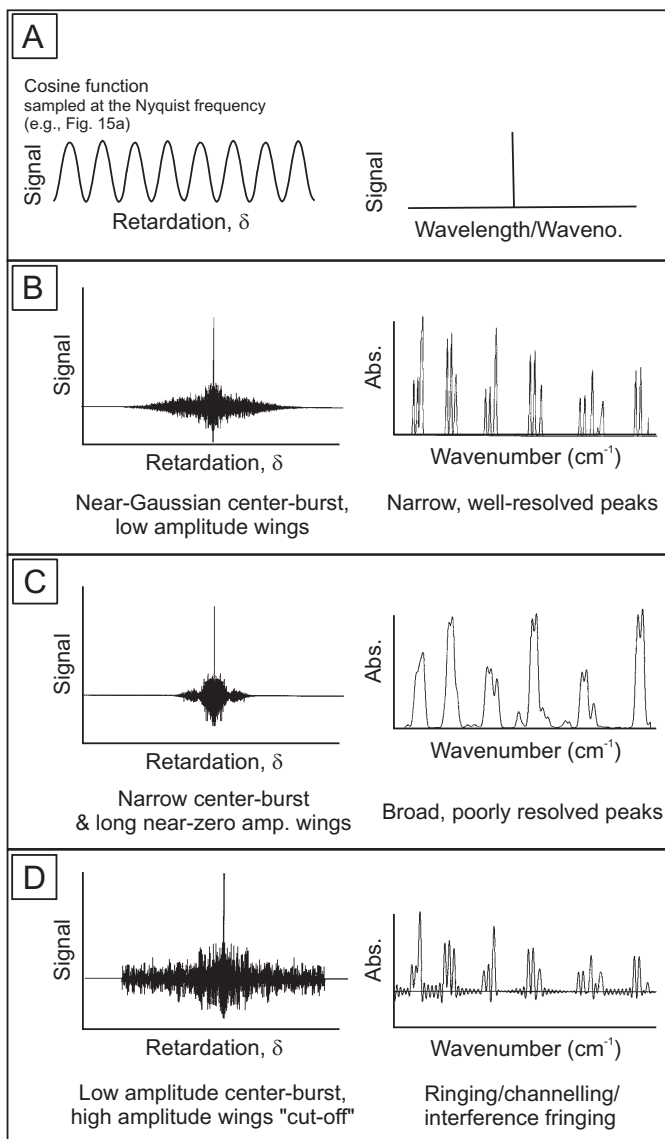
Interferogram   Fourier Transformation

A

Cosine function
sampled at the Nyquist frequency
(e.g., Fig. 15a)

Signal

Retardation, δ

Signal

Wavelength/Waveno.

B

Signal

Retardation, δ

Near-Gaussian center-burst,
low amplitude wings

Abs.

Wavenumber (cm⁻¹)

Narrow, well-resolved peaks

C

Signal

Retardation, δ

Narrow center-burst
& long near-zero amp. wings

Abs.

Wavenumber (cm⁻¹)

Broad, poorly resolved peaks

D

Signal

Retardation, δ

Low amplitude center-burst,
high amplitude wings "cut-off"

Abs.

Wavenumber (cm⁻¹)

Ringing/channelling/
interference fringing

FIG. 3-15: A) Cosine function sampled at the Nyquist frequency and the accompanying Fourier transformation showing a single peak with no peak width. B) Gaussian-shaped interferogram that becomes relatively near-zero on the wings. The Fourier Transformation shows a spectrum of the nitrogen molecular ion near 23,400 cm^{-1} (~0.43 µm); C) A relatively short interferogram with sharp trunkations and an accompanying Fourier Transformation spectrum of the nitrogen molecular ion near 23,400 cm^{-1} showing relatively broad lines; D) An interferogram with a sharp cutoff before it reaches zero amplitude. The accompanying spectrum of the nitrogen molecular ion near 23,400 cm^{-1} shows ringing and reduced spectral resolution. Note that some spectral resolution may have been lost in modifying the figure from Davis *et al.* (2001).

artifacts in the Fourier transform procedure. Typical apodization functions are shown in Table 3-3. It is beyond the scope of this chapter to go into details of other apodization functions (*e.g.,* see Davis *et al.* 2001,Griffiths & de Haseth 1986, Lynn & Fuerst 1998).
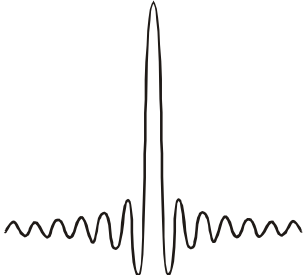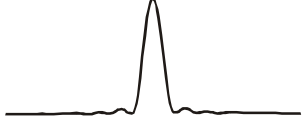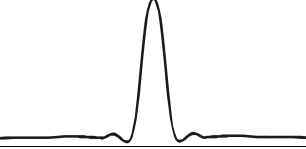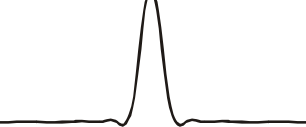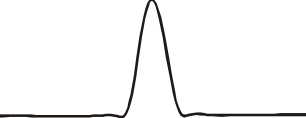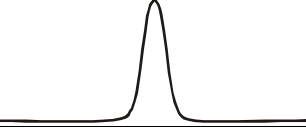
The challenge is to choose an apodization function that does not inappropriately modify the band shape in the process of minimizing the Fourier Transform problems. In practice, this is most important where one is measuring narrow vibrational bands (such as those encountered in gas phase spectroscopy) or where one is trying to accurately fit bands. For example, the function may overcorrect for the side lobes resulting in difficulties in defining the width and area of the IR band and possibly interfering with bands that are close together. Alternately, the apodization procedure may overcorrect for the instrument line shape, which affects the full-width at the half-

maximum height of the band, FWHM. Table 3-3 shows that there is generally a trade-off between side lobe minimization and improved line shape. Apodization functions with "sharp edges" such as the Boxcar function result in Fourier Transformed spectra with reduced reliability (Table 3-3).

TABLE 3-3 - APODIZATION FUNCTIONS

Function	Function equation D(x)	Transform F{D(x)} versus x	Instrument line shape	FWHM	Amplitude of largest side lobe (rel. %)
Boxcar	$D(x) = 1$ $|x| \leq L$, 0 $|x| > L$		$2L \sin c(2\pi vL)$	1.207 /2L	-21%
Trapezoidal	$2D(x) \cdot [1 - (|x|/L)] - D(2x) \cdot [1 - (2|x|/L)]$		$2L \sin c^2(\pi vL) - 0.5\sin c^2(\pi vL/2)$	1.546 /2L	-15%
Triangular	$D(x) \cdot [1 - (|x|/L)]$		$2L \, sinc(2\pi vL)$	1.772 /2L	+4.5%
Triangular squared	$D(x) \cdot [1 - (|x|/L)]^2$		$4L/(2\pi vL)^2) \cdot [1 - sinc(2\pi vL)]$	2.359 /2L	+0.7%
Bessel	$D(x) \cdot [1 - (|x|/L)^2]^2$		$16(\pi/2)^{0.5}L/ (2\pi vL)^{2.5} \cdot J_{2.5}(2\pi vL)]$	1.904 /2L	-4.1%
Cosine	$D(x) \cdot 0.5[1 + (\cos(\pi x/L)]$		$[\sin c(2\pi vL)]/ [2\pi v(1-4L^2v^2)]$	2.000 /2L	-2.7%
Sinc^2	$D(x) \cdot sinc^2(\pi x/L)$		$2L[\sin c(2\pi vL)] \cdot [L(1-|L|v)]$	2.174 /2L	-1.0%
Gaussian	$D(x) \cdot \exp[- (\pi^2/ln2) \cdot (x/2L)^2]$		$2L [ln2^{0.5}/\pi^{0.5}] \cdot \exp[-(2vL)^2 ln2]$	2.030 /2L	-0.45%

Aliasing

The position of the moving mirror in the interferometer is determined by using a reference He-Ne laser beam (Fig. 3-1, Fig. 3-5b), from this perspective, the frequency of the laser beam monitors the maximum sampling frequency. If too few sample points are taken in a spectrum, then non-existent bands may appear in the interferogram, but are replicated in the Fourier Transform by a process known as <u>aliasing</u> (Figure 3-16a-d). This problem occurs where the sampling frequency for a monochromatic wave is such that more than one frequency wave is possible (*e.g.*, sine wave shown in Figs. 3-17b, c). A common example of this phenomenon is the view that wheels on cars appear to spin backwards in movies that have been sampled at certain frame frequencies.

For instance, if a sine wave is sampled at twice its frequency it can be defined unambiguously (Fig. 3-17a). However, if the sampling frequency is not at twice the frequency of the wave (Figs. 3-17b, 3-17c), then the frequency of the wave is ambiguous. To determine the minimum number of sample points, N_s, in a spectral range (max to min), the following equation is used (also known as the <u>Nyquist criterion</u>):

$$N_s = 2(\tilde{v}_{max} - \tilde{v}_{min})/\Delta\tilde{v} \qquad (5)$$

(Griffiths & de Haseth 1986). To minimize aliasing problems it is recommended that the user examine only the portion of the spectrum necessary to minimize the $\tilde{v}_{max}$ - $\tilde{v}_{min}$ term.

Interference ringing or fringing

The sample thickness is related to the refractive index of the sample and the wavelength of interest via the equation:

$$2n\text{d} = \text{m}\lambda \qquad (6)$$

where, n is the refractive index, d is the sample thickness and m is an integer (1, 2, 3, etc.). For transmission spectroscopy, if the sample is thicker than the wavelength of interest (*e.g.*, >10 microns thick at $\tilde{v}$ = 1000 cm^{-1} or λ = 10 μm), then the spectrum may have interference fringes related to multiple reflections in the sample producing constructive and destructive interference. Changing the sample thickness is one method to minimize interference fringes: generally it is easiest to thin or wedge the sample.

In some cases, it is possible to increase the spectral resolution of sample collection until ringing vanishes in the noise. Generally to minimize ringing, at least three samples per FWHM are required for a Lorentzian band, or at least five samples per FWHM for a Gaussian band (Davis *et al.* 2001, also see Hirschmugl 2004).
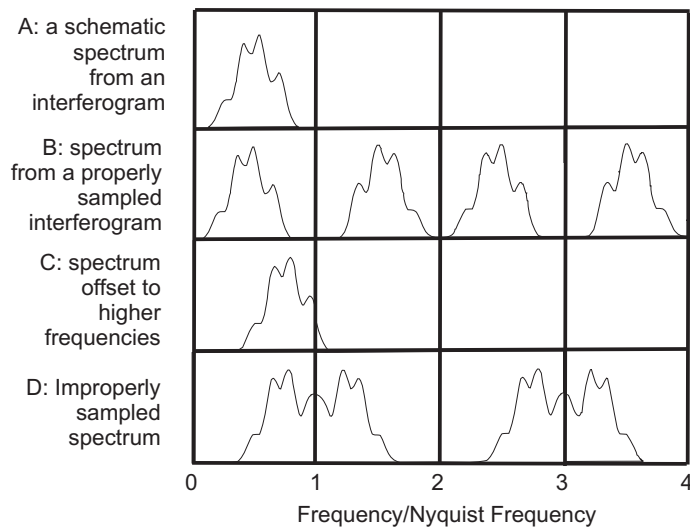

FIG. 3-16: Example of band aliasing showing A) a schematic spectrum from an interferogram; B) spectrum from a properly sampled interferogram, showing non-overlapping aliases; C) the same spectrum, but moved to higher

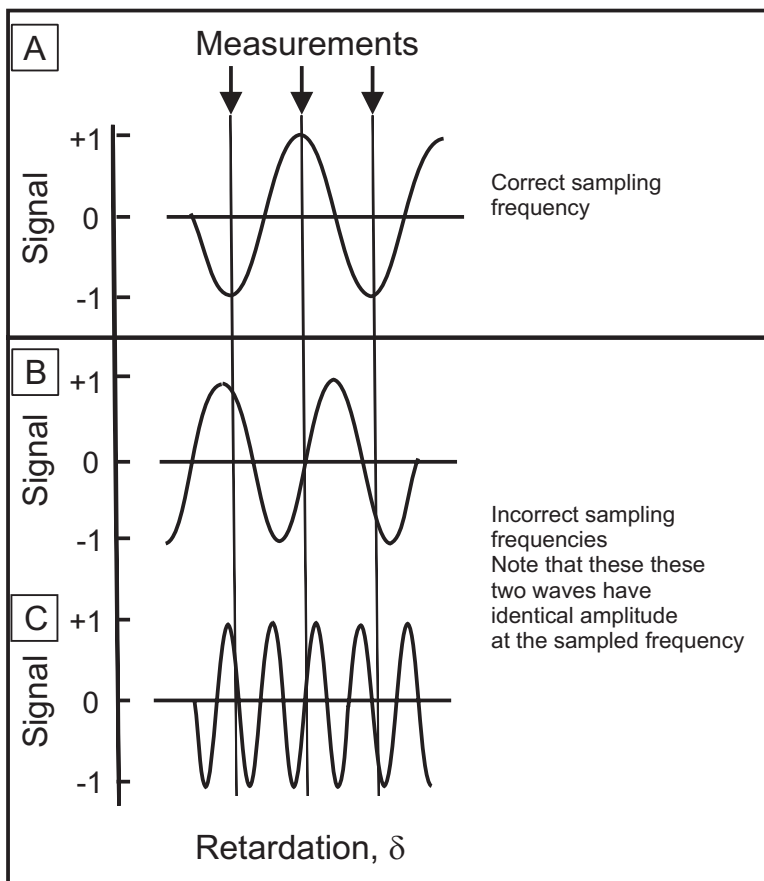frequencies; D) spectrum from the improperly sampled interferogram.

FIG. 3-17: Example of how band sampling should be frequent enough to define the frequency of the wave. A) the wave has been sampled correctly at exactly twice its frequency (Nyquist criterion). Relative to the wave in a, a lower frequency wave in B) is not sampled correctly and neither is a higher frequency wave in C). Both B) and C) have the same amplitude at the sampling frequency.

Another method to minimize ringing is to apply an apodization function to the interferogram so that its amplitude at a distance from the centerburst is minimized (Table 3-3) (Davis *et al.* 2001). In Figure 3-15b, the centerburst and wings have a near-Gaussian shape that results in a spectrum with little ringing and well-defined bands. In contrast, in Figures 3-15c and d, there are discontinuities (sharp edges) in the spectra that result in poor quality spectra. In Figure 3-15c, the interferogram has resolvable intensity for a relatively small retardation distance from the centerburst resulting in broad, poorly resolved bands. In Figure 3-15d, the wings of the interferogram have high intensity that rapidly drops off causing a sharp discontinuity in the data resulting in ringing. Although apodization improves ringing, it does affect the band shapes (as discussed above).

TRANSMISSION IR SPECTROSCOPY
Qualitative transmission analysis

An IR transmission spectrum is measured as percent transmission (T %) of the IR beam through the sample as a function of the wavenumber (or wavelength). The transmission function is defined as $T = I_{trans}/I_0$, where I_0 is the IR intensity incident on the sample, and I_{trans} is that transmitted through the sample (Fig. 3-9a). Dips in transmission occur at or near the frequencies of IR active vibrational modes of the sample (Fig. 3-9a).

If the analyst is interested in "finger-printing" organic compounds (*e.g.*, pharmaceutical products), it is useful to be able to examine all bands present as a percentage: %T. The percentage scale has the advantage of highlighting small bands and is particularly useful for band height ratio techniques. However, %T is not a linear function of concentration; instead, it is necessary to use

absorbance, A (Fig. 3-9b).

Quantitative transmission analysis

For absorption spectra, the <u>Bouger-Beer-Lambert Law</u> links the concentration of species in a particular IR band (c, in moles), the transmission function (I_{trans}/I_0), and absorbance (A in absorbance units) following:

$$A = \ln (I_{trans}/I_0) = \varepsilon\, c\, d \qquad (7)$$

where ε is the extinction coefficient ($mol.L^{-1}cm^{-1}$), d is the sample thickness (Fig. 3-9a). To minimize error in A, it is best to measure absorbance units between 0.2 and 1.2 units (Fig. 3-9c) due to the increased possibility of non-linear detector response beyond this range.

The <u>integrated intensity</u>, $\bar{A}$, is more sensitive than the linear intensity, A, and is defined as:

$$\bar{A} = (1/cd) \int \ln(I/I_0)_{\tilde{v}}\, d\tilde{v} = \int \varepsilon^*_{\tilde{v}}\, d\tilde{v} \qquad (8)$$

where $\varepsilon^*_{\tilde{v}}$ is the integrated extinction coefficient for the band. The integrated intensity is best to use in cases where the band shape or width changes with increasing concentration of the sample. However, it should be noted that for narrow bands (*e.g.*, gases) the integrated intensity is dependent on the apodization function used (discussed above).

It is generally good practice to prepare samples so that the transmission is >80 % in wavelength ranges away from strong IR bands of the sample, and dips to no less than ~10 % at the absorption band (transmission minimum) of interest. If the latter condition is not met, then the transmission minimum will appear very broad and will have a "flattened" top, making it difficult to define the band position, because of the nature of the transmission function and its relationship to the IR absorption spectrum. These conditions can be realized by varying the concentration of sample contained within the disc, to increase the absorption intensity due to the band of interest.

The <u>baseline</u> (Fig. 3-9b) can be adjusted by carefully preparing the disc for study: anomalous baseline values can appear due to light scattering effects caused by discs that contain grain boundaries and air pockets that have not been pressed out. Various types of baselines may be used to fit spectra (Fig. 3-9b).

REFLECTANCE SPECTROSCOPY

Types of analyses possible with reflection spectroscopy

1) Specular reflectance (also known as <u>external reflection spectroscopy</u> or <u>ERS</u> or <u>bidirectional reflectance</u>) uses an incident IR beam at an air/sample interface (Figs. 3-2, 3-10), the angle of the incident IR light equals the angle of reflectance. This technique has the advantage in that it is nondestructive and limited sample preparation is required. Specular reflectance spectroscopy works best for samples with a high refractive index (*e.g.*, Fig. 3-7).

The penetration distance into sample is poorly known and is a function of the sample surface (*e.g.*, surface preparation), properties of the sample (*e.g.*, density, refractive index), and the angle of the incident light. Because the penetration depth is commonly ~$10^0 – 10^1$ microns the surface greatly affects the spectrum.

To quantify the spectra, the reflectance of the sample is measured relative to a background using a mirror such as Au, stainless steel or Al. Bands may show unusual "sigmoidal shapes" (Fig. 3-2) that require Kramers-Kronig transformation (below). As indicated in Clark (2004), some industries use log(1/R) data, but this is not quantitative because it is depends on the scattering process of the particles.

2) Diffuse reflectance Fourier Transform infrared spectroscopy is also known as <u>DRIFTS</u> or <u>DR</u> in materials science, and <u>biconical reflectance</u> in the remote sensing community (Hapke 1993). IR radiation is focused on a spherical or ellipsoidal focusing mirror then scattered, absorbed, transmitted and reflected by the sample and then back onto the mirror (Figs. 3-2, 3-10). Background spectra are collected using a mirror that is spectrally flat. Samples are placed in a cup (~13 mm diameter x 2 mm deep) or a micro-sampling device (3 mm diameter x 2mm deep). To achieve a random orientation of grains to minimize polarization effects it is necessary to sift the sample into the holder. In some cases, baffles on the diffuse reflectance unit may interfere with the beam path, resulting in poor signal and the reader is referred to Clark *et al.* (2003) for a detailed discussion of such cases.

For quantification of samples with small total absorption, DRIFTS spectra may be converted to <u>Kubelka-Munk (KM) units</u> following:

$$KM = (1 - R_\infty)^2 / 2R_\infty = k' / s \qquad (9)$$

where, R_∞ = specular reflectance from an infinitely thick sample, k' = DRIFTS absorption, s = scattering factor. This conversion is carried out because it converts reflectance, which is a nonlinear function of absorbance, to a quantity that is linear relative to absorbance, provided the absorbance is small.

Another approach that is used commonly in the remote sensing community is to convert the spectra using <u>Hapke Theory</u> or <u>Mie Theory</u> or variations of these. In contrast to Kubelka-Munk theory, Hapke Theory accounts for samples with large total absorption (*e.g.*, many minerals and mineral mixtures; Clark & Roush 1984). These approaches are beyond the scope of this chapter and more detailed discussions are provided in Hapke (1993) and Clark (2004).

3) *Directional-hemispherical reflection* is performed to best simulate the scattering of energy over a complete hemisphere, or where comparison to non-directional emissivity using <u>Kirchhoff's Law</u> (see below) is required. The most common approach for acquiring these spectra is to use an integrating sphere coated with a surface that is diffusely reflective to the IR radiation (*e.g.*, gold). The set-up of integrating spheres is variable, however most attach to an external port in the spectrometer, through which the collimated energy passes. The sphere diameter can also vary and generally it is determined as a function of the desired sample and beam spot size. For example, a 12.7 cm sphere with a 2.5 cm opening will focus a 1.5 cm spot size on the sample (Salisbury *et al.* 1991). A measurement is made of the sphere with the sample replaced by a cover with the same gold coating and curvature of the sphere. The energy of the near-perfect reflector is captured by the detector assembly, which is external to the sphere and at 90° to the principle plane of the incident energy. The sample is placed at the opening to the sphere and illuminated. The reflectance collected is ratioed against the reflectance from the sphere alone in order to determine the absolute reflectance of the sample alone. Non-hemispherical reflectance from the sample is minimized by baffling the detector assembly so as not to view the sample directly. The data are treated in the same manner as for diffuse reflectance.

4) *Attenuated total reflection* involves transmitting the IR beam through a crystal that has a moderately high refractive index (n_c, Fig. 3-2), such as ZnSe (Fig. 3-7) which results in near-total internal reflection. This technique is also called <u>internal reflection spectroscopy (IRS)</u>. The properties of the crystal result in a standing wave, known as an evanescent wave, that has a <u>depth of penetration</u> (DP) of typically a few microns into the sample, dependent on the refractive index of the sample (n_s), n_c, ν, angle of incidence (θ):

$$DP^{-1} = (2\,\pi\,\nu\,n_c) * \{\sin\theta^2 - (n_s / n_c)^2\}^{1/2} \qquad (10)$$

Because penetration depth is inversely dependent on ν, at low ν the DP is larger than at high ν, resulting in more intense absorption at low ν. Also, n_c affects DP and absorption, for instance, samples in contact with diamond ATR crystals (n_c = 2.44-2.41, Fig. 3-7) will have greater DP and absorption intensity than samples in contact with Ge ATR crystals (n_c = 4 – 4.1). Similarly, varying θ will also change DP. An advantage of changing DP (by changing n_c or θ) is that it is possible to find a <u>depth profile</u> in a sample. Another advantage of ATR is that aqueous solutions may be analyzed because the short wavelengths mean that H_2O is not totally absorbing; this is advantageous for geomicrobiology studies as long as the samples do not react with the ATR crystal. Micro-ATR is a technique that is rapidly gaining popularity. In this technique, the ATR crystal is mounted on a microscope attachment. It is useful to use a diamond ATR crystal because many minerals are hard and scratch both Ge and ZnSe crystals (Fig. 3-7, Knoop hardness).

Theoretical introduction and practical considerations- specular reflectance

In this section we discuss methods for quantifying such data where the source and the detector are highly collimated because this is the set-up commonly available in the laboratory setting. In contrast, reflectivity measurements at non-normal incidence, or using a detector and/or source with a lesser degree of collimation are encountered in remote sensing and require considerably more complicated data treatment (*e.g.*, Hapke 1993, Clark & Roush 1984, Clark 2004).

A normal-incident specular reflectance spectrum contains detailed information on the optical constants of the material, including the variation of the real and imaginary parts of the

refractive index (n(ν) and k(ν), or n'(ν), n''(ν)), or the dielectric parameter (ε'(ν), ε''(ν)) and the absorption coefficient ($\alpha(\nu) = 4\pi\nu k(\nu)$) (Decius & Hexter 1977, Hapke 1993, McMillan 1984, McMillan & Hofmeister 1988). A specular reflectance spectrum obtained from a single flat sample surface at normal incidence can thus be analyzed to obtain the IR absorption spectrum, as well as valuable additional information such as the variation of the refractive index (n) with wavelength in the IR region (*e.g.*, Grzechnik *et al.* 1996, Moore *et al.* 2000).

As discussed in Clark (2004), the reflectivity of a sample is related to the frequency dependent refractive index (n(ν)) of the material at normal incidence *via* the Fresnel relation:

$$R = \left(\frac{|n-1|}{|n+1|}\right)^2 \tag{11}$$

As discussed above, reflectivity measurements at non-normal incidence are treated with considerably more complicated equations (Hapke 1993).

The "high-frequency" refractive index (the "R.I.") measured in the visible range is usually determined by the interaction of light with the electron density in the sample, far from any vibrational or electronic resonances: values of the R.I. are generally well-correlated with the glass density. The refractive index is correlated with the dielectric parameter (ε) via the relation:

$$\varepsilon = n^2 \tag{12}$$

At frequencies approaching zero, the refractive index is related to the static dielectric constant ε_o. From these relationships, the optical constants of a material (*i.e.*, n(ν) and ε(ν)) can be determined from a measurement of the reflectivity, R(ν). In most materials, resonances occur in the infrared region between IR-active vibrational modes and the propagation of light through the material that result in anomalous dispersion, and the need to consider both real and imaginary parts to n(ν) and ε(ν)

$$n(\nu) = n_1 + in_2 \tag{13a}$$

$$\varepsilon(\nu) = \varepsilon_1 + i\varepsilon_2 \tag{13b}$$

(Hadni 1967, McMillan 1984, McMillan & Hofmeister 1988, Burns 1990, Efimov 1995). Equation 12 becomes

$$\varepsilon_1^{\;2} = n_1^{\;2} - n_2^{\;2} \tag{14a}$$

$$\varepsilon_2 = 2n_1 n_2 \tag{14b}$$

The imaginary part of the refractive index ($n_2(\nu)$: also termed k(ν) or n''(ν) in some treatments) or the dielectric function ($\varepsilon_2(\nu)$ or ε''(ν)) is directly related to the IR absorption coefficient by:

$$\alpha(\nu) = 4\pi\nu n_2 \tag{15}$$

In order to determine α(ν) from reflectivity data, it is usual to analyze the reflectivity function either *via* an empirical fitting procedure based upon modeling the data with a series of damped harmonic oscillators (discussed in Hofmeister 2004), or using an analytic method termed a Kramers-Kronig analysis, that is based upon linear response theory (Hadni 1967, McMillan 1984, McMillan & Hofmeister 1988, Burns 1990, Efimov 1995).

In the Kramers-Kronig procedure, the real and imaginary parts of the frequency dependent refractive index are related to the measured reflectance by the equations:

$$n_1(\nu) = \frac{1 - R(\nu)}{1 + R(\nu) - 2\sqrt{R(\nu)}\cos\Theta(\nu)} \tag{16a}$$

$$n_2(\nu) = \frac{-2\sqrt{R(\nu)}\sin\Theta(\nu)}{1 + R(\nu) - 2\sqrt{R(\nu)}\cos\Theta(\nu)} \tag{16b}$$

where R(ν) is the measured reflectance function, ν is the frequency (given in wavenumber units), and the loss function $\Theta(\nu)$ to be determined from the measured reflectivity data is given by the integral relation:

$$\Theta(\nu) = -\frac{1}{2\pi}\int_0^\infty \log\left[\frac{\nu + \nu*}{|\nu - \nu*|}\right]\frac{d\log R(\nu*)}{d\nu*}d\nu* \tag{17}$$

In this expression, ν is the frequency value at each point considered, and ν* is the integration variable. Evaluation of Θν leads to determination of the optical constants of the material, $n_1(\nu)$ and $n_2(\nu)$, or $\varepsilon_1(\nu)$ and $\varepsilon_2(\nu)$ through equations 13a-b. With n_1 and n_2 thus determined, we can then calculate the absorption coefficient (α) as a function of frequency using the relation (equation 15) given above and for direct comparison with values obtained from transmission experiments (*e.g.*, Moore *et al.* 2000). Various forms of the Kramers-Kronig relationships

(equations 15, 16a, 16b) can be derived (*e.g.*, Efimov 1995), and the spectroscopist can choose that which is most amenable to numerical calculation, and that gives the most stable solution.

In order to apply equation 17 to calculate $\Theta\nu$ and thus obtain the optical constants including the absorption coefficient (equation 15), it is necessary to have information on the experimental reflectivity function at both the low- and high-wavenumber limits, as $\nu \to 0$ and as $\nu \to \infty$. In practice this is not possible. Even an approximation to this condition requires considerable experimental effort, and even then, approximate solutions must be sought. As the optical constants are investigated to high frequencies, the contribution to the reflectivity function from vibrational excitations becomes minimal above the wavenumber range of fundamental IR-active vibrations, *i.e.*, above approximately 4000 cm^{-1} (or below 2.5 μm wavelength range). Although contributions from overtones and combination modes do occur above this value, they are very weak, and they contribute little to the refractive index. The primary contribution to $n(\nu)$ throughout most of the visible to near-IR range is due to the <u>electronic polarizability</u>, before the onset of the resonances due to electronic transitions in the visible-UV range. The "high frequency" limiting value for n_∞ and R_∞ is thus often taken to be the refractive index measured in optical microscopy studies of glasses (and minerals), for analysis of their reflectivity in vibrational investigations. In the low frequency limit, the $R(\nu\to0)$ value is often estimated from capacitance measurements of the <u>static dielectric constant, ε_o</u> (Burns 1990, Efimov 1995). An appropriate function must then be chosen to link that low frequency limiting R_o value with the onset of the measured $R(\nu)$ spectrum, that begins at a wavenumber determined by the instrumental configuration. In micro-beam FTIR studies of most silicate glasses and minerals, the instrumental set-up is with a Globar source, KBr beam splitter and MCT-A detector, thus the low frequency cutoff is at approximately 450 cm^{-1} (~22 μm). Thus some bands are neglected, which alters the <u>phase angle</u> (the angle of reflection).

Comparison of reflectance and emission spectroscopy

To determine whether a material reflects IR radiation producing reflectance spectra or acts as a blackbody source producing emission spectra, it is necessary to determine the emission factor, ε_K by applying <u>Kirchhoff's Law</u>:

$$\varepsilon_K = 1 - R \qquad (18)$$

where $\varepsilon_K = 1$, the material is a black body source. Kirchhoff's Law has been successfully applied to relate <u>biconical reflectance IR (DRIFTS)</u> to <u>non-directional emittance</u> spectra (Lyon 1965). However, if the emissivity is <u>directional</u> (the emitted radiation is measured at a given direction, *e.g.*, due to the sun's location) then Kirchhoff's Law (equation 18) is valid only if the reflectance is either <u>hemispherical-directional</u> (Fig. 3-10) or <u>directional-hemispherical</u> (Fig. 3-10) and the sample is observed or illuminated from the same direction (for more details see Hapke 1993, Clark & Roush 1984, Clark 2004, Clark *et al.* 2003).

EMISSION SPECTROSCOPY

Infrared emission spectroscopy (ε-FTIR) is closely related to the previous discussion of reflectance spectroscopy. The spectral features arising from the fundamental, combination, and overtone vibrational bands are present, appear as troughs or emissivity lows rather than reflectance peaks (Lyon 1965, Hapke 1993). For a large range of particle sizes and emission (viewing) angles, this relationship between R-FTIR and ε-FTIR is complimentary and described using Kirchhoff's Law (equation 18). Further, neither reflection and emission spectroscopy require the sample preparation nor handling involved in transmission measurements, nor is diffractive scattering an issue.

The fundamental difference between the reflectance and emission techniques is the source of the infrared energy. In emission spectroscopy, the sample itself becomes the infrared source: in order to observe a signal *via* IR emission, it is necessary that the sample be at a different temperature to that of the IR spectrometer system (*i.e.*, the ensemble of optics and detector, along with the "standard" used to determine the intrinsic response of the system), and/or that it have a different wavelength-dependent emissivity function ($\varepsilon(\lambda)$) in the spectral region of interest. Thus, this technique is best for inorganic solids, such as minerals and amorphous materials on planetary surfaces, but it is impractical for other samples (*i.e.*, ices, many organic materials).

However, emission spectroscopy is the most directly comparable to IR remote sensing measurements and therefore collection of spectra by that means may be critical depending on the application (see below).

Emission measurements at elevated temperatures

Although an emission signal is not restricted to materials heated to high temperatures, typically this is the most practical method for emission analysis because the sample signal is greater and it is easier to differentiate from the instrument signal. Recently Ruff *et al.* (1997) gave a complete description of a laboratory design for gathering and calibrating quantitative ε-FTIR spectroscopy.

The sample, spectrometer, and environment are commonly at differing temperatures and therefore radiating different amounts of blackbody energy (Fig. 3-3). These can be described by the equation2 (Planck's Law) modified by the wavelength-dependant emissivity of each component. These blackbody energies must be accounted for and removed in order to derive the emissivity of the sample. The most basic approach used to solve for sample emissivity and remove the effects of temperature and instrument energy is the two-temperature method (Christensen & Harrison 1993). In this approach the sample and the blackbody sources are measured at two different radiating temperatures in order to solve for the wavelength-dependent emissivity [ε(λ)] of the sample:

$$\varepsilon(\lambda) = [E_s(T_{2,\lambda}) - E_s(T_{1,\lambda})] / [E_{bb}(T_{2,\lambda}) - E_{bb}(T_{1,\lambda})]$$
(19)

where, E_s and E_{bb} are the energies of the sample and blackbody, each radiating at two different temperatures (T_1 and T_2). This methodology is difficult to perform experimentally for several reasons: a) it requires the same temperature for the sample and the blackbodies, b) upper microns of a geologic material may emit at a different temperature than the bulk of the sample, c) there may be complications due to radiative cooling of the optical surface resulting in thermal gradients, d) maintaining the instrument and environmental temperature during the measurements and collecting four spectra per sample is cumbersome, and e) in some cases, the temperature is not directly measured, instead the radiance is collected resulting

in assumptions regarding conversions from radiance to temperature.

A more convenient laboratory approach is to use two heated blackbody emitters, which are maintained at different temperatures that bracket the sample temperature (*e.g.*, 70° and 100°C). The blackbodies are each measured once for calibration, which allows the instrument response function (containing the emission of the bench instrument's components) to be quantified and removed from subsequent sample measurements. In addition, an environmental chamber that emits blackbody energy at a precise temperature (*e.g.*, 25°C) is used to house the sample during data collection. This mitigates emitted energy from the surrounding environment, which could reflect off the sample and enter the beam path to the detector. Finally, an actively regulated heat source may be used to maintain the sample temperature during long spectra acquisitions (*e.g.*, 80 - 90°C).

However, as with any measurement of radiant flux from a natural surface, acquiring spectra at only one temperature produces an under-determined set of equations. At each wavelength the radiance is a function of the sample temperature and the wavelength-dependant emissivity. In other words, a spectrum with 100 spectral points (and therefore 100 distinct measurements of radiance) would have 101 unknowns: 100 emissivity values and one radiating temperature. The determination of these unknowns must be done by making an assumption about either one of the emissivity values or the surface temperature, or by introducing extra data such as laboratory-derived spectra (Kahle 1987, Realmuto 1990, Hook *et al.* 1992). Of the various permutations on separation of emissivity from temperature, typically it is most straight-forward to use the normalized emittance technique similar to that described by Christensen (1982) and Realmuto (1990). The basic assumption of the model is that at some point in the spectrum of the sample there is a maximum emissivity value at or near unity (*e.g.*, Christiansen frequency), although the wavelength of this maximum is not specified. Using the assumed emissivity to solve equation 2 (Planck's Law) at the wavelength of maximum radiance, yields the derived temperature of the sample. This temperature can then be used to solve equation 2 again, however this time for the emissivity at every wavelength. And although an assumption is made in separating temperature from

emissivity, the precise radiating temperature of the sample is known and the error small where compared to trying to measure the sample at two different temperatures under identical conditions (*e.g.* equation 19). This method is convenient for materials with large grain sizes and no thermal gradient (*e.g.*, Christensen *et al.* 2000) and works best for single-component samples (*e.g.*, MgO, Hofmeister *et al.* 2003). In theory, multicomponent samples may be problematic due to variable chemical environments for the atoms resulting in variable Christiansen frequencies and deviation of the emissivity from one. However, in practice most naturally occurring mixtures, have Christiansen frequencies in similar wavelength regions. Further, separation of emissivity from temperature at the Christiansen frequency is done over a range of values (*e.g.* 100 wavenumber) and therefore errors arising from multicomponent mixtures are minimized.

The approaches to measuring ε-FTIR outlined above are valid as long as the instrument and/or environmental temperature do not vary significantly (<1-2°C) during the collection of sample spectra (Ruff *et al.* 1997). Because emission spectra must be normalized to temperature, temperature stability of the system is critical for calibration, as well as precision and accuracy of laboratory emissivity measurements (*e.g.*, Ruff *et al.* 1997).

Another factor that affects precision and accuracy is the SNR. Relative to T-FTIR and R-FTIR, ε-FTIR has a low signal that results in a relatively low SNR. To increase SNR, commonly multiple scans of a sample are co-added (see Table 3-2 and discussion above) and it is most advantageous to use a high sensitivity detector (*e.g.*, MCT-A). Increasing the number of scans results in a higher likelihood for temperature fluctuations and these two variables must be carefully balanced.

Advantages of emission IR spectroscopy

The question arises however as to why a laboratory emission spectroscopy design would be favored over that of R-FTIR spectroscopy. There are several important factors to consider where deciding between ε-FTIR and R-FTIR spectro-scopy. First, collection of ε-FTIR spectra is by definition hemispherically-integrated radiance and thus eliminates most of the angular dependencies that arise in reflectance spectroscopy. Collection in

this mode more accurately mimics the emission from natural surfaces where observed by remote sensing instruments. For example, where examining coatings and particular particle orientations. Certain particle/crystal orientations as well as thin coatings may produce spectral emissivity features not apparent where using hemispherical reflectance spectroscopy. Second, emission of infrared radiance is what naturally occurs on the Earth's surface and therefore laboratory-based measurements are directly comparable to remote sensing data. The average surface temperature of the Earth (~25°C) produces a maximum emitted flux at 9.7 μm, whereas at wavelengths longer than ~5 μm, the solar reflected energy approaches zero. Therefore, no reflected IR energy is observed at values larger than 5 μm (*e.g.*, Sabins 1987). In such situations, only emission spectra can be gathered by field-, air- or space-based instruments. Third, the examination of spectral features at wavelengths greater than 25 μm. For planetary applications, where obscuration by the atmosphere long ward of ~12 μm is not a problem, emission spectroscopy provides the only means of examining the spectral features of minerals at these wavelengths. The energy from reflectance sources falls off dramatically after 25 μm and hence lowers the SNR markedly. Finally, the cost must be considered. Whereas it can be expensive to fabricate the custom hardware needed for an emission spectrometer design, the cost of a 13 cm gold-coated integrating sphere can exceed $20,000 (US). However, the complexity of acquiring the spectra and the need to heat the sample, generally preclude most laboratories from performing emission spectroscopy. Typically, the aforementioned caveats are minor for most researchers and reflection spectra are collected and converted to emissivity by way of Kirchhoff's Law (equation 18).

Remote emission IR spectroscopy

Emitted energy from each pixel within remotely-acquired data can treated as the emitted radiance collected from a sample in the laboratory. However, unlike the controlled conditions of the laboratory, remotely acquired emissivity must be corrected for the intervening atmospheric column, which scatters, absorbs, and re-emits IR energy. The additional radiance added by the atmosphere can generally be accurately removed using one of

several atmospheric correction algorithms (*i.e.*, MODTRAN) that rely on assumption about the volume and distribution of IR-active atmospheric gas species (*i.e.*, CO_2, H_2O, and O_3) and aerosols (Berke *et al.* 1989). A second important difference between laboratory and remotely-acquired emission spectra is the methodology of instrument calibration. One or two near-ideal black body source(s) are carried within most IR remote sensing instruments. Typically, the instrument scans one blackbody at a high temperature, then a line of data in the scene, and then the second blackbody at a lower temperature. This two-point calibration can be used to quantify the instrument response function, monitor instrument drift during data collection, and be used as a two point calibration from which to extract surface emissivity on a pixel by pixel basis. However, the accuracy and stability of the onboard blackbodies must be carefully monitored (Realmuto *et al.* 1995).

CONCLUSIONS

There are three main types of FTIR spectroscopy: transmission, reflectance and emission analysis. Each technique uses similar instrumentation, but the results and techniques differ.

Transmission techniques provide optimal information on the absorbance of samples with small quantities of molecular species, and this technique is best for thin samples or finely ground powders. Transmission techniques may be used for studies where polarization is an issue. Another advance of T-FTIR is that absorbance values are relatively easy to interpret (Bouger-Beer-Lambert law, equation 7).

Reflectance IR is advantageous for a variety of sample types (films, powders, alloys). There are a variety of attachments that can be used to facilitate analysis using R-FTIR. A disadvantage of R-FTIR is that reflectance data is complicated to interpret due to variations in the refractive index with wavelength resulting in data treatment using a variety of methods (*e.g.*, Kubelka-Munk, Kramers-Kronig or Hapke analysis).

Emission IR is advantageous for remote sensing coarse-grained samples (>100 µm). The technique has the advantage of ease of use, particularly in the natural environment or using remote platforms. However, the technique is challenging in the laboratory due to low SNR and the need for temperature stability.

In evaluating FTIR spectrum it is important to consider the media in the beam path such as atmospheric background, windows and carriers. It is also necessary to understand the artifacts that may arise due to changing the spectral resolution, SNR, instrument gain and Fourier Transformation methods. Hopefully this chapter and the accompanying references provide an outline of some of the important variables.

REFERENCES

BERKE, A., BERNSTEIN, L.S., & ROBERTSON, D.C. (1989): MODTRAN: A moderate-resolution for LOWTRAN 7, *Geophys. Lab., Air Force Syst. Command, Rep. GL-TR-89-0122*, Hanscom Air Force Base, Mass., 38.

BERNER, E.K. & BERNER, R.A. (1996): *Global Environment: Water, Air, and Geochemical Cycles*. Prentice Hall, Upper Saddle River, NJ.

BURNS, G. (1990): *Solid State Physics*. Academic Press, London.

CANIOU, J. (1999): *Passive Infrared Detection: Theory and Applications*. Kluwer Academic Publ., Boston.

CAPPER, P. & ELLIOTT, C.T. (eds.) (2000): *Infrared Detectors and Emitters: Materials and Devices*. Kluwer Academic Publ., Boston.

CHRISTENSEN, P.R. (1982): Martian dust mantling and surface composition: Interpretation of thermophysical properties. *J. Geophys. Res.* **87**,

9985-9998.

CHRISTENSEN, P.R. & HARRISON, S.T. (1993): Thermal-infrared emission spectroscopy of natural surfaces: Application to desert varnish coatings on rocks. *J. Geophys. Res.* **98** 19819-19834.

CHRISTENSEN, P. R., BANFIELD, J. L., HAMILTON, V. E., HOWARD, D. A., LANE, M. D., PIATEK, J. L., RUFF, S. W., & STEFANOV, W. L. (2000): A thermal emission spectral library of rock-forming minerals. *J. Geophys. Res.* **105**, 9735-9739.

CLARK, R.N. (2004): Spectroscopy of rocks and minerals, and principles of spectroscopy. In *Infrared Spectroscopy in Geochemistry, Exploration Geochemistry and Remote Sensing* (P.L. KING, M.S. RAMSEY, G.SWAYZE, ed.), Mineral. Assoc. Canada, Short Course **33**, 17-55.

CLARK, R.N. & ROUSH, T.L. (1984): Reflectance spectroscopy: Quantitative analysis techniques for remote sensing applications. *J. Geophys. Res.* **89**, 6329-6340.

CLARK, R.N., SWAYZE, G.A., WISE, R., LIVO, K.E., HOEFEN, T.M., KOKALY, R.F., & SUTLEY, S.J. (2003): USGS digital spectral library splib05a. *U.S. Geol. Surv. Open-File Report 03-395.* (http://pubs.usgs.gov/of/2003/ofr-03-395/ofr-03-395.html)

CROWLEY, J.K. (2004) Hydrothermal mineral zoning within an eroded stratocone: Remote sensing spectral analysis of Brokeoff Volcano, California. In *Infrared Spectroscopy in Geochemistry, Exploration Geochemistry and Remote Sensing* (P.L. KING, M.S. RAMSEY, G.SWAYZE, ed.), Mineral. Assoc. Canada, Short Course **33**, 215-226.

DAVIS, S.P., ABRAMS, M.C., & BRAULT, J.W. (2001): *Fourier Transform Spectrometry*. Academic Press, San Diego.

DECIUS, J.C. AND HEXTER, R.M. (1977): *Molecular Vibrations in Crystals*. McGraw-Hill, New York.

DERENIAK E. L. & BOREMAN G.D. (eds.) (1996): *Infrared Detectors and Systems*. John Wiley & Sons.

EFIMOV, A.M. (1995): *Optical Constants of Inorganic Glasses.* CRC Press, Boca Raton.

FARMER, V.C. (1974, ED.): *The Infrared Spectra of Minerals,* Mineral. Soc. London, 539.

GRIFFITHS,P.R. & DE HASETH, J.A. (1986): *Fourier Transform Infrared Spectrometry*. John Wiley & Sons, New York.

GRZECHNIK, A., ZIMMERMANN, H.D., HERVIG, R.L., KING, P.L., & MCMILLAN, P.F. (1996): FTIR micro-reflectance measurements of the CO_3^{2-} ion content in basanite and leucitite glasses. *Contrib. Mineral. Petrol.* **125**, 311-318.

HADNI, A. (1967): *Essentials of Modern Physics Applied to the Study of the Infrared*. Pergamon.

HANNAH, R.W. (1988): Introduction to data processing and sources of error. In *Advances in Applied Fourier Transform Infrared Spectroscopy* (ed. MACKENZIE, M.W.) John Wiley & Sons, New York, 1-42.

HAPKE, B. (1981): Bidirectional reflectance spectroscopy. 1. Theory. *J. Geophys. Res.* **86**, 3039-3054.

HAPKE, B. (1993): *Theory of Reflectance and Emittance Spectroscopy*. Cambridge Univ. Press, Cambridge.

HAWTHORNE, F.C. & WAYCHUNAS, G.A. (1989): Spectrum-fitting methods, In *Spectroscopic Methods in Mineralogy and Geology* (ed. HAWTHORNE, F.C.) *Rev. Mineral.* **18,** Mineral. Soc. Am., Blacksburg, VA, 63-98.

HENINI, M. & RAZEGHI, M. (eds.) (2002): *Handbook of Infrared Technologies*. Elsevier Science Ltd.

HIRSCHMUGL, C.J. (2002a): Frontiers in infrared spectroscopy at surfaces and interfaces. *Surf. Sci.* **500**, 577-604.

HIRSCHMUGL, C.J. (2002b): Applications of storage ring infrared spectromicroscopy and reflection-absorption spectroscopy to geochemistry and environmental science In *Applications of synchrotron radiation in low-temperature geochemistry and environmental sciences* (eds. FENTER, P.A, RIVERS, M.L., STURCHIO, N.C., SUTTON, S.R.) *Rev. Min. Geochem.,* **49**: Mineral. Soc. Am. & Geochemical Soc., Washington DC, 317-339.

HIRSCHMUGL, C. (2004): An Introduction to

Infrared Spectroscopy for Geochemistry and Remote Sensing. In *Infrared Spectroscopy in Geochemistry, Exploration Geochemistry and Remote Sensing* (P.L. KING, M.S. RAMSEY, G.SWAYZE, ed.), Mineral. Assoc. Canada, Short Course **33**, 1-16.

HOFMEISTER, A.M. (2004): Thermal and thermodynamic properties from infrared spectra. In *Infrared Spectroscopy in Geochemistry, Exploration Geochemistry and Remote Sensing* (P.L. KING, M.S. RAMSEY, G.SWAYZE, ed.), Mineral. Assoc. Canada, Short Course **33**, 135-154.

HOFMEISTER, A.M. & ROSSMAN, G.R. (1985): A model for the irradiative coloration of smoky feldspar and the inhibiting influence of water. *Phys. Chem. Minerals* **12**, 324-332.

HOFMEISTER, A.M., KEPPEL, E. & SPECK, A.K. (2003): Absorption and reflection IR spectra of MgO and other diatomic compounds. *Monthly Notices Royal Astron. Soc.* **345,** 16-38.

HOOK, S.J., GABELL, A.R., GREEN, A.A., & KEALY, P.S. (1992): A comparison of techniques for extracting emissivity information from thermal infrared data for geologic studies. *Rem. Sens. Environ.* **42**, 123-135.

HUNT, G.R. (1976): Infrared spectral behavior of fine particulate solids. *J. Phys. Chem.* **80**, 1195-1198.

JHA, A.R. (2000): *Infrared Technology: Applications to Electrooptics, Photonic Devices and Sensors*. John Wiley & Sons.

KAHLE, A.B. (1987): Surface emittance, temperature, and thermal inertia derived from thermal infrared multispectral scanner (TIMS) data for Death Valley, California. *Geophy.* **52**, 858-874.

KEMPFERT, K.D., SHIFU, W., LEIMER, B., & PETTY, C. (na): Performance features of an extended range beam splitter for mid- and near-IR spectroscopy. *Nicolet Technical Note* (TN-9583).

KEPPLER, H. & RAUCH, M. (2000): Water solubility in nominally anhydrous minerals measured by FTIR and ^{1}H MAS NMR: the effect of sample preparation. *Phys. Chem. Minerals* **27**, 371-376.

KING, P.L., MCMILLAN, P.F. & MOORE, G.M.

(2004): Infrared spectroscopy of silicate glasses with application to natural systems. In *Infrared Spectroscopy in Geochemistry, Exploration Geochemistry and Remote Sensing* (P.L. KING, M.S. RAMSEY, G.SWAYZE, ed.), Mineral. Assoc. Canada, Short Course **33**, 93-133

KOKORINA, V.F. (1996): *Glasses for Infrared Optics*. CRC Press, Boca Raton.

LEIMER, B. & KEMPFERT, K. (na): Optimizing optical bench performance for near-IR and visible spectroscopy. *Nicolet Technical Note* (TN-9580).

LYNN, P.A. & FUERST, W. (1998): *Introductory Digital Signal Processing with Computer Applications*. John Wiley, New York.

LYON, R.J.P. (1964): Evaluation of infrared spectrophotometry for compositional analysis of lunar and planetary soils, Part II: Rough and powdered surfaces, *Stanford Res. Inst., NASA-CR-100,* Washington, D.C.

LYON, R.J.P. (1965): Analysis of rocks by spectral infrared emission (8 to 25 microns), *Econ. Geol.* **60**, 715-736.

MCMILLAN, P.F. (1984): Structural studies of silicate glasses and melts- applications and limitations of Raman spectroscopy. *Am. Mineral.* **69**, 622-644.

MCMILLAN, P.F. & HOFMEISTER, A. (1988): Infrared and Raman Spectroscopy, In *Spectroscopic Methods in Mineralogy and Geology* (ed. HAWTHORNE, F.C.) *Rev. Mineral.* **18**, Mineral. Soc. Am., Blacksburg, VA, 99-159.

MCMILLAN, P.F. & WOLF, G.H. (1995): Vibrational spectroscopy of silicate liquids. In *Structure, dynamics and properties of silicate melts.* (ed. STEBBINS, J. F., MCMILLAN, P. F & DINGWELL, D. B.) *Rev. Mineral.*, **32**, Mineral. Soc. Am. Washington DC, 247-315.

MICHAELIAN, K.H. (2003): *Photoacoustic Infrared Spectroscopy*. Anal. Chem. & its Appl. Series (ed. WINEFORDNER, J.D.) John Wiley & Sons.

MOERSCH, J.E. & CHRISTENSEN, P.R. (1995): Thermal emission from particulate surfaces: A comparison of scattering models with measured spectra. *J. Geophys. Res.* **100**, 7465-7477.

MOORE, G., CHIZMESHYA, A. & MCMILLAN, P.F.

(2000): Calibration of a reflectance FTIR method for determination of dissolved CO_2 concentration in rhyolitic glass. *Geochim. Cosmochim. Acta* **64**, 3571-3579.

MUSTARD, J.F. & HAYS, J.E. (1997): Effects of hyperfine particles on reflectance spectra from 0.3 to 25 μm. *Icarus* **125**, 145-163.

NAFIE, L.A. (1988): Polarization modulation FTIR spectroscopy. In *Advances in Applied Fourier Transform Infrared Spectroscopy* (ed. MACKENZIE, M.W) John Wiley & Sons, New York. 67-104.

RAMSAY, D.A. (1952): Intensities and shapes of infrared absorption bands of substances in the liquid phase. *J. Am. Chem. Soc.* **74**, 72-80.

RAMSEY, M.S. & CHRISTENSEN, P.R. (1998): Mineral abundance determination: Quantitative deconvolution of thermal emission spectra, *J. Geophys. Res.* **103**, 577-596.

REALMUTO, V.J. (1990): Separating the effects of temperature and emissivity: Emissivity spectrum normalization. In *Proceed. 2nd Ann. Airborne Earth Science Workshop* (ed. ABBOTT, E.A.*) JPL Publ.* **90-55**, 31-35.

REALMUTO, V.J, HAJEK, P., SINHA, M.P., & CHRIEN, T.G. (1995): The 1994 laboratory calibration of TIMS. In *Summaries 5th Ann. Airborne Earth Science Workshop* (ed. REALMUTO, V.J) *JPL Publ.* **95-1**, 25-28.

RIVARD, B., GALLIE, E.A. & FENG, J. (2004): Estimating chalcopyrite and pyrrhotite/ pentlandite in ores of the Sudbury Mines using visible and infrared spectroscopy. In *Infrared Spectroscopy in Geochemistry, Exploration Geochemistry and Remote Sensing* (P.L. KING, M.S. RAMSEY, G.SWAYZE, ed.), Mineral. Assoc. Canada, Short Course **33**, 241-251

ROSSMAN, G.R. (1988a): Vibrational spectroscopy of hydrous components. In *Spectroscopic Methods in Mineralogy and Geology* (ed. HAWTHORNE, F.C.) *Rev. Mineral.* **18**, Mineral. Soc. Am., Blacksburg, VA 193-206.

ROSSMAN, G.R. (1988b): Optical Spectroscopy. In *Spectroscopic Methods in Mineralogy and Geology* (ed. HAWTHORNE, F.C.) *Rev. Mineral.* **18**, Mineral. Soc. Am., Blacksburg, VA 207-254.

RUFF, S., CHRISTENSEN, P.R., BARBERA, P.W., & ANDERSON, D.L. (1997): Quantitative thermal emission spectroscopy of minerals: a laboratory technique for measurement and calibration. *J. Geophys. Res.* **102**, 14899-14913.

SABINS, F.F. (1987) *Remote Sensing: Principles and Interpretation.* Freeman, New York.

SALISBURY, J.W. & WALD, A. (1992): The role of volume scattering in reducing spectral contrast of reststrahlen bands in spectra of powdered minerals. *Icarus* **96**, 121-128.

SALISBURY, J.W., WALTER L.S., VERGO N., & D'ARIA D.M. (1991): *Infrared (2.1 - 25 mm): Spectra of Minerals*. Johns Hopkins University Press, Baltimore.

SCHRADER, B. (1995): *Infrared and Raman Spectroscopy: Methods and Applications*, VCH, Weinheim, Germany.

SMITH, B. (1996): *Fundamentals of Fourier Transform Infrared Spectroscopy*. CRC Press, Boca Raton.

SMITH, B. (1999): *Infrared Spectral Interpretation: A Systematic Approach*. CRC Press, Boca Raton.

SWAYZE, G.A., CLARK, R.N., GOETZ, A.F.H., CHRIEN, T.G. & GORELICK, N.S. (2003): Effects of spectrometer band pass, sampling, and signal-to-noise ratio on spectral identification using the Tetracorder algorithm. *J. Geophys. Res.* 108(E9), 5105, doi:1029/2002JE001975, 30 p.

VAN DER MAREL, H.W. & BEUTELSPACHER, H. (1976): *Atlas of Infrared Spectroscopy of Clay Minerals and their Admixtures*. Elsevier, Amsterdam

VINCENT, R.K. & HUNT, G.R. (1968): Infrared reflectance from mat surfaces. *Appl. Optics* **7**, 53-59.

WENRICH, M.L. & CHRISTENSEN, P.R. (1996): Optical constants of minerals derived from emission spectroscopy: Application to quartz, *J. Geophys. Res.* **101,** 15921-15931.

WOLFE, W.L. & ZISSIS, G.J. (1985): *The Infrared Handbook*. Office of Naval Research, Department of the Navy, Washington DC.

APPENDIX 3-1: CHECKLIST FOR SETTING UP AN IR SPECTROSCOPY LAB

Room
- Dust-filtered environment to minimize maintenance on fans in power supplies
- Low vibrations to aid machine alignment and mirror movement
- Minimal temperature fluctuations to improve detector performance
- Minimal drafts and humidity to improve background reproducibility
- A high-pressure dry air line is useful if a purge system will be used
- Steady power supply and low radiation noise are optimal

Furniture and computing supplies
- Tables and chairs for spectrometer and sample preparation
- For some applications (e.g., far IR) it is advantageous to purchase an air table with low vibration levels for the spectrometer
- Storage cabinet(s) for spectrometer parts, accessories and samples
- Computer with data backup hardware and a printer
- Nearby telephone for trouble-shooting and safety issues

Spectrometer accessories
- Dry air (CO_2-scrubbed) and/or N_2 purge

Maintenance and data storage
- Maintenance manual for spectrometer
- Log book to keep track of analyses and instrument performance

Microscope accessories
- Plate with polished Au, stainless steel or Al for reflectance
- 100 µm pin hole for aligning the instrument

Sample preparation materials
- Digital camera for photographing samples, linked to computer
- Furnace for drying samples (<1000 ºC)
- Sample flattening devices: sieves, spatulas, rollers
- Grinding and cutting equipment
- Small sample devices: (vacuum) tweezers
- Sampling accessories: diamond cell, ATR, grazing angle objective
- Pellet-making equipment: KBr die and vacuum press, IR lamp, ~100 °C oven
- Weighing balance sensitive to ~10^{-5} g

APPENDIX 3-2: PERFORMANCE & MAINTENANCE CHECKLIST

To better monitor a laboratory IR spectrometer, it is helpful to record the following information (outlined in detail in Smith, 1996):

Source signal amplitude (max. voltage of the interferogram "centerburst") - this is an indication of the IR radiation reaching the detector. If the source signal varies by more than a few percent it may indicate that the source is damaged, vibrating, ending its useful lifetime, or fluctuating in temperature. Some researchers monitor the centerburst amplitude before doing each analysis to ensure that there is sufficient signal; we generally use an arbitrary minimum of 3 volts for quantitative analyses.

Source signal location is a measure of the interferometer performance and if it varies by a large amount there are likely problems with the interferometer (vibrations, mirror velocity errors or problems with the He-Ne laser).

Beam splitter behavior should be monitored regularly by examining a background spectrum for a given spectrometer. The ratio of the intensity at the background cutoff at high wavenumber is a measure of spectrometer performance. For example, in Figure 6, the value for the ratio is calculated using the maximum intensity (I_{max} ~38) and the intensity at 4000 cm^{-1} (~2.5 µm; I_{4000} ~9) to calculate:

$$\text{beam splitter \%} = I_{4000} / I_{max} \sim 24\,\% \tag{20}$$

Because the spectrum is expected to behave like a black body this slope should be relatively shallow, but the absolute value will depend on the spectrometer efficiency. If the beam splitter % decreases the beam splitter may have deteriorated (e.g., fogged) or may need realigning.

Spectrometer noise should be monitored regularly by taking two background spectra sequentially to produce a spectrum that should have close to 100% transmittance, with a slight slope, noise, and atmospheric bands. The resulting spectrum will be curved if there is a misalignment of the beam splitter. The slope should be relatively low over the spectral range (<1 %) dependent on the spectrometer, beam splitter, spectral resolution, source and number of scans. The noise can be measured band-to-band in a region away from the atmospheric bands (e.g., 2100-2200 cm^{-1} region; 4.5-4.8 µm).

Variables to monitor regularly

Spectrometer resolution
The effective resolution (precision) of a spectrometer is determined by measuring FWHM for a gas with inherently narrow bands (e.g., CO). For example, if a gas has FWHM = 0.1 cm^{-1}, but the measured FWHM is 1 cm^{-1}, then the effective resolution of the spectrometer is 1 cm^{-1}. Because the laser might drift, the accuracy of the wavenumbers may be monitored using the major band in polystyrene film (1601 cm^{-1}; Smith, 1996).

Purge
The purge performance is checked examining atmospheric CO_2 and H_2O bands in a background. The desiccant level can also be checked. Generally, maintenance on the purge is limited to changing the purge filter(s).